SILICIDE FUEL SWELLING BEHAVIOR AND ITS PERFORMANCE IN I2S-LWR

A Thesis
Presented to
The Academic Faculty

By

Matias G. Marquez

In Partial Fulfillment
Of the Requirements for the
Degree Master of Science in Nuclear Engineering

Georgia Institute of Technology

[August, 2015]

SILICIDE FUEL SWELLING BEHAVIOR AND ITS PERFORMANCE IN I2S-LWR

Approved by:

Dr. Bojan Petrovic
Nuclear and Radiological Engineering
Georgia Institute of Technology

Dr. Abderrafi Ougouag
Idaho National Laboratory

Dr. Chaitanya Deo
Nuclear and Radiological Engineering
Georgia Institute of Technology

Date Approved: July 17, 2015

ACKNOWLEDGEMENTS

The author of this thesis is thankful to everyone who made this work possible with their support and companionship. In special I would like to mention some important people.

To Dr. Bojan Petrovic for his advisory during the pursue of my degree and his confidence that I was up to the task he proposed to me.

To Dr. Abderrafi Ougouag for his mentorship and constant guidance during the development of this thesis and his hospitality during my stays in Idaho.

To Idaho National Laboratory for providing me a place to work on the research that concluded with this thesis.

To Dr. Chaitanya Deo who was part of the reading committee together with Dr. Petrovic and Dr. Ougouag.

To my family for their support from the distance.

And finally to Programa BEC.AR and Fulbright who funded me to be able to come to this university to pursue my degree and to the DOE Office of Nuclear Energy for partially funding my research through the Nuclear Energy University Programs (NEUP).

TABLE OF CONTENTS

LIST OF TABLES

LIST OF FIGURES

SUMMARY

The swelling mechanisms of U_3Si_2 under neutron irradiation in reactor conditions are not unequivocally known. However, the limited experimental evidence that is available suggests that the main driver of swelling in this material would be the accumulation of fission gas at crystalline grain boundaries. The steps that lead to the accumulation of fission gases at these locations are multiple and complex. At first, when fissions occur, the fission products, including volatile and gaseous ones, would be deposited mostly within crystalline grains. In this state, gas atoms behave essentially as a solute in solution or as clusters of few gas atoms forming primitive bubbles that would occupy available volume between the constituent atoms of the crystal thus causing little swelling, in magnitude comparable to the swelling caused by solid fission products. However, gradually, the gaseous fission products migrate by diffusion. Upon reaching a grain boundary, which acts as a trap, the gaseous fission products start to accumulate, thus leading to formation of bubbles and hence to swelling.

The mechanisms described above, in addition to depending on their various respective driving forces, also depend on the proximity of grain boundaries. Thus, for very large grains, diffusing fission gases may not reach the boundary and remain, effectively, in

solution or in the form of clusters of a few gas atoms. It follows that the formation of bubbles would be enhanced by the proximity of grain boundaries, i.e., by small initial grain sizes or by the subdivision of large grains into numerous small ones.

Prior to irradiation, the material under consideration, U_3Si_2, is assumed to be composed of relatively large grains. Therefore, a quantitative model of swelling requires the incorporation of phenomena that increase the presence of grain boundaries and decrease grain sizes, thus creating sites for bubble formation and growth. Following Rest [1], it is assumed that new grain boundary formation results from the conversion of stored energy from accumulated dislocations into energy for the formation of new grain boundaries. The model, thus, must include the movement of various atomic species as well as climb and rearrangement of dislocations into cellular structures.

This thesis develops a quantitative model for grain subdivision in U_3Si_2 based on the above mentioned phenomena to attempt to infer or verify the presence of this mechanism, which when used in conjunction with computational codes, that model allows the evaluation of the total swelling of a fuel pellet in a reactor environment over the fuel lifetime.

Because of the scarcity, or even nearly total absence, of experimental data on U_3Si_2 swelling behavior under reactor operating conditions, the model is validated using known and estimated data and parameters for UO_2 and comparing predicted results to experimental trends of high burnup structures in this latter material. Finally, the model is used to generate predictions for U_3Si_2 performance with the understanding that given the

large uncertainties about the applicable parameters for this material and the lack of calibration experimental evidence, the predictions are to be used with great caution and should be subjected to future comparisons and corrections when the necessary data become available.

Although the model developed is intended to be useful in a wide range of conditions, the analysis of the results will be focused in the typical conditions of PWR. The temperature of validity will be above critical amorphization temperature.

This thesis is organized as follows, Chapter 1 explains the motivation of this work, Chapter 2 provides an introduction of concepts necessary to understand the physics behind the model, Chapter 3 introduces the concept of swelling and explains its different causes, Chapter 4 discusses the different models that explain gaseous swelling, Chapter 5 details the model developed for this thesis, Chapter 6 describes the methodology by which the results were obtained, Chapter 7 displays the results and interprets them, Chapters 8 and 9 provide further analysis of the impact of the results in the fuel performance and Chapter 10 contains the conclusion.

CHAPTER 1

Introduction

Overview

In recent years, nuclear power experienced a resurge of interest as a source of clean energy, useful to reduce CO_2 emissions. However, the low price of fossil fuels and new safety concerns which arose after the Fukushima-Daiichi events led to an emphatic interest both in increasing the profitability of the electricity produced and in reducing the risk of accidents.

In this context, and with these goals, the I^2S-LWR reactor project was initiated. This project proposed a preliminary design that includes considerations for making the reactor inherently safe, and for trying to avoid or minimize risk to its output and efficiency.

Nuclear power plants generate energy by means of nuclear fissions. The energy is deposited primarily as heat within the fuel, with a small fraction carried by neutrons and gamma radiation to the coolant, the vessel, and structural materials. The heat is subsequently removed by the coolant and then transported (usually) into a traditional thermal cycle that generates electrical energy.

This brief description provides evidence of the centrality of the nuclear fuel and its design to the functioning of a nuclear reactor. In particular, safety performance is to a great extent governed by the behavior of the fuel.

In the most typical configuration, such as that of light water reactors, the fuel material, in the form of short cylindrical pellets, is contained within cylindrical rods, the outermost shell of which is termed the cladding. The rods are arranged in parallel "bundles" or "assemblies." The collection of all assemblies constitutes the "core" or innermost part of a nuclear reactor. Within the rods, between the pellets and the cladding there normally exists a small region dubbed the gap.

Different materials have been developed for use both as the pellet and as the cladding. The most extensively used fuel material is uranium dioxide (UO_2), but other options are UN, UC and, in the case of I^2S-LWR, U_3Si_2 [2].

As can be surmised, the system pellet-gap-cladding constitutes a complex structure that affects, within less than an inch in the radial direction, the performance of the entire reactor. There exists a varied palette of interconnected effects, properties and parameters that act over, and influence, this system, the most significant of which is thermal conductivity of its constitutive elements. The latter property dominates the phenomena that govern the temperature profile across the pellet. Of course, the temperature profile is also affected significantly by the total power level, which is determined primarily by neutronics. If the power is kept constant, deterioration of the thermal conductivity would

induce an increase of the fuel temperature, especially at the pellet centerline, exposing it to the risk of melting, a highly undesirable situation.

Within a fuel element, the most resistive region to heat transfer is the gap. Resistivity obviously depends to a great extent on the gap width. A low resistivity would imply better heat transfer and hence improved overall efficiency while maintaining fuel centerline integrity, therefore one would favor a narrow gap design. Conversely, a narrow gap implies a smaller space into which to collect volatile fission products and into which a swelling pellet may expand, thus limiting the level of burnup that could be reached. These conflicting demands are usually addressed by a fine balancing design act: incorporate the smallest gap that accounts for the expected swelling of the pellet and is capable of accommodating the volatile species and, conversely, select and/or design the material of the pellet to minimize swelling while allowing as high a burnup level as possible. The mechanisms that have to be accounted for in this design optimization process include all causes for pellet dimensional change through pellet lifetime. Such causes may include thermal expansion (volume increase), densification (volume decrease) and radiation-induced swelling (volume increase). The driving reasons for some of the constraints mentioned above pertain to fuel and fuel cladding integrity: excessive swelling can cause the fuel to contact the cladding and possibly imposing stresses on the latter and ultimately inducing it to fail.

The present thesis reports on a model that has been created for modeling the mechanisms underlying the radiation-induced swelling of fuel pellets. The model can be used to

support the design of pellet gap width by modeling the dimensions change of the pellet over its lifetime in the reactor under operating reactor conditions.

I^2S-LWR features

The I^2S-LWR is a NEUP-DOE funded project that involves the participation of national and international universities, national laboratories and industrial entities [2]. As mentioned above, its preliminary design includes safety considerations to reduce the risk of accidents through passive systems and minimize human intervention in the event of an accident, without reducing the plant's profitability and hence maintaining economic attractiveness.

Safety considerations include features such as passive decay heat removal and the use of cladding which does not generate hydrogen even under accident conditions, thus avoiding the concomitant explosion risk [3]. This new cladding, made of stainless steel, introduces a neutronic penalty which must be compensated for in some way. Hence, the I^2S-LWR reactor postulates a new fuel material to be used: U_3Si_2. U_3Si_2 presents a higher uranium density than UO_2, enabling longer cycles despite the cladding penalty. The high thermal conductivity is also an attractive feature of the fuel. Reducing the thermal gradient along the pellet and lowering the centerline temperature, the safety is improved as the maximum temperature will be far from the melting temperature [4].

U_3Si_2 has already been used in research reactors, but such reactors' operating conditions and configuration are completely different from those anticipated to prevail in the I^2S-

LWR reactor. There follows, some uncertainty on the expected material performance of the proposed fuel. The principal issue of concern is the observed swelling in irradiated U_3Si_2. Experience had shown that the dimensional change of U_3Si_2 fuels can largely exceed the expected swelling levels considered acceptable for a fuel to be used in a nuclear power reactor (versus use in research reactors). However, these measurements have been performed only in research reactor conditions, which are far from the conditions of the I^2S-LWR design, making them inconclusive for this fuel material under power reactor conditions.

The objective of this thesis is to obtain a comprehensive model to predict the swelling of U_3Si_2 fuels subjected to irradiation under PWR conditions. The results presented here will be useful as a baseline for the determination of the acceptability of U_3Si_2 as a fuel for the I^2S-LWR reactor and, in case of a positive result, for the design of the related fuel element.

CHAPTER 2

Theoretical background

Material science considerations

Before initiating the development of the propose model of this thesis, some concepts related to solid state physics must be presented. To begin with, solid materials can be classified in different ways, from which we must highlight two: composition and atomic order and structure.

If materials should be divided according to their composition, the main groups would be metals, ceramics, polymers, composites, semiconductors and biomaterials. From those, only metals and ceramics (and comparable materials) are of interest for this work. Metallic materials are composed of one or more metal elements. On the other hand, ceramics are constituted of compounds of metallic and non-metallic elements [5]. While according to this classification, UO_2 can be clearly considered a ceramic, the metalloid nature of Si (dual behavior between metal and non-metal) makes unclear the proper classification of U_3Si_2. Although it is sometimes called an intermetallic compound [6, 7], we will still treat it as a ceramic, unless some specific distinction could be made.

Most of the materials in the previous groups (especially metals and ceramics) can also be classified according to their atomic structure; if long-range ordered, periodic

arrangements are repeated all over the material, they are termed *crystalline*; if long-range periodicity of the arrangement is not present, the material is called *amorphous* [5].

This distinction is particularly important for this work as theories exist that assume that swelling occurs because of the behavior of bubbles in an amorphous material, while others state that bubbles nucleate and grow in a polycrystalline structure. As the model chosen for this thesis is the swelling caused by gas behavior in a crystalline structure, some material notions are necessary to understand what is occurring while the material is under irradiation.

Microstructural analysis of crystalline and amorphous materials give different pictures, mainly because of the existence of fixed positions at which atoms are located on crystals as they bond to the neighboring atoms, with defined distances between their respective positions and with the requirement of precise energy input for any modification to this arrangement, while this is not completely correct in amorphous materials. This ordered long-range array is called a lattice and it is defined by the unit cell, which is the basic structural volume that repeats all along the crystal [5].

Unit cell shape and size depend on the material (although the same material can present different structures under different conditions). In general terms, these cell shapes can be described as parallelepipeds or prisms with three sets of parallel faces. Most common crystal structures, according to the configuration of their unit cell are cubic (simple, faced-centered or body-centered), hexagonal, tetragonal (simple or base-centered), orthorhombic (simple, base-centered, face-centered or body-centered), triclinic and

monoclinic (simple or base-centered). However, the classification can be much more complicated than this, especially for compound materials.

The crystalline structure of UO_2 is the very common face-centered cubic (FCC) known as the fluorite because it matches the structure of CaF_2, though with different lattice parameter. The fluorite structure consists of two FCC sub-lattices that are offset from one another, while, however, keeping the alternation of atoms needed to preserve electronic neutrality. The crystalline structure of U_3Si_2 cannot be described that easily; atoms are arranged in tetragonal cells in which U cations have two different valence states with each valence state at a different location in the cell structure, while Si atoms are present in pairs (Si_2) that occupy a single atom site [8, 9].

As stated above, a crystalline material is a long-range periodic arrangement of atoms that ideally repeats all over the crystal. However, perfect crystals do not exist. For example, in polycrystalline materials (i.e., materials formed by more than one crystal grain), a boundary exists between grains and the long-range arrangement is discontinued at that grain boundary.

Statistically, in thermal equilibrium, imperfections called point defects appear in the microstructure of crystalline materials. These defects can either be vacancies or interstitials. A vacancy is a defect consisting of the absence of an atom from its normal site, while an interstitial consists of an atom located between normal crystal sites. Vacancies appear more often than interstitials due to energetic considerations. This thermal equilibrium is a dynamic equilibrium; vacancies and interstitials can recombine

and be consumed, causing a recovery of the regular atom lattice structure, while new pairs of vacancies and interstitials can also be created.

Point defects can also be created by radiation damage. When energetic particles collide with the material atoms, they can transfer enough energy to break the bonds that keep the atoms in their respective places and displace some of them from their regular lattice site. If this event occurs isolated, a pair of a vacancy and an interstitial would be created. However, that which often occurs (mainly during irradiation with high energy heavy ions) is a cascade of displacements where a large number of point defects are produced. Most of these defects recombine again at a determinate recombination rate depending on the temperature, but some of them do survive increasing the steady state concentration of defects to a level that is usually higher than the thermal equilibrium concentration by several orders of magnitude [10].

Other important microstructural components are the defect sinks. There exist different types of sinks. Among the most common sinks one could count grain boundaries, dislocations, voids and bubbles. In simple situations, sinks can be static, of constant concentration and inexhaustible. Sinks are also characterized by the rate at which point defects react with them, a phenomenon sometimes quantified by a parameter dubbed the sink strength. Sinks, if they are significant and strong, affect the equilibrium concentration of the point defects. Point defect evolution in simple model can be represented by the following differential equations:

$$\frac{dC_v}{dt} = Q_v - K_{iv}C_vC_i - K_{vs}C_vC_s \quad (1)$$

$$\frac{dC_i}{dt} = Q_i - K_{iv}C_vC_i - K_{is}C_iC_s \quad (2)$$

where C_v is the concentration of vacancies, C_i is the concentration of interstitials, the first term of both equations indicates the production rate of each species, the second term stands for the recombination and the third one for the annihilation at sinks with C_s denoting the concentration of sinks. Unfortunately, many material engineering problems do not conform to these simplifications, thus adding complexity [10, 11].

The main assumption made in the previous model statement is the absence of space gradients, equivalent to stating that defects are homogeneously distributed. This will not be completely true in most cases, but generally this can be used as a good approximation. Although diffusion under concentration gradients is neglected, there are different ways to compensate for it by considering its effect within the rate constants (e.g. the calculation of the sink strength includes the effect of spatial gradients on it but the latter are not explicitly modeled in separate equations).

The types of sinks mentioned above are also named extended defects that, in contrast to point defects, extend along two or three dimensions. Sometimes, average values can be used for the density or concentration of these defects. However, in some cases that is not a realistic assumption, and their evolution must be studied together with the evolution of point defects as the respective behavior of the extended and the point defects are interrelated.

While vacancy and interstitial concentrations proper are not usually related directly to actual macroscopic material properties, extended defects do play a major role in establishing mechanical properties. Yet, for this work, each type of defect is recognized as a contributor in its own different, way to the swelling of the pellet. Thus, the understanding of their respective effect on, or contribution to, swelling, requires that their nature be understood.

Dislocations are one-dimensional, or linear, defects around which atoms are misaligned [5]. Dislocations can be of different types: edge, screw or mixed. An edge dislocation is a half-plane of atoms inserted between two planes of the lattice. This extra half plane terminates inside the crystal, causing a distortion of the crystal structure around the termination line, also known as dislocation line [5]. Screw dislocations, in contrast, can be thought of as the distortion caused by application of localized shear stress to a plane of the crystal, resulting in a shift of a line of atoms laying in that plane by one atomic distance in that plane [5].

Usually, dislocations have a more complex structure, including a mixture of edge and screw dislocations (mixed type). Every dislocation is characterized by a vector called Burgers Vector. This vector can be understood as follows. If a close loop is drawn in a perfect lattice and then a dislocation is added, the loop will not be closed anymore. The Burgers vector is the vector that closes that loop.

More explanatory material on the behavior of dislocations will be presented later; however as an introduction it can be said that as dislocations pile up they form subgrains,

which may later, singly or in aggregates, form subdivided grains. The walls that divide the grains into subgrains are usually considered low-angle grain boundaries (LAGB) as each such wall separates adjacent regions that make slightly different angles with it, i.e., the wall separates subzones with small relative lattice misorientations. This configuration of dislocations, piled up and forming walls surrounding subgrains, is named a dislocation network. Grain subdivision plays a very important role in the study of swelling, as subdivision would create additional grain boundary surfaces.

Grain boundaries are surface, or two-dimensional, defects. They can be described as sudden changes in the orientation of the planes in which lattice sites are arranged. The misorientation between grains tends to be large; therefore they are named high-angle grain boundaries (HAGB). They have properties that are different from those of the core of the grains. Mainly, and of direct interest to this work, they provide a more stable location for bubbles to grow.

Bubbles are an example of three-dimensional defects. As commonly understood or conceptualized, they are "pockets" of gas surrounded by bulk material. Bubbles are one of the main drivers of swelling in fuels. As bubbles grow, material is displaced and there results an increase of the dimension of the fuel pellet.

Radiation damage

As described in equations (1) and (2), the evolution of the concentration of both types of point defects of interest can be described in terms of a rate theory, in a way similar to that

adopted for chemical reactions, where rate constants are defined that quantify the frequency with which reactions occur and are multiplied by the concentrations involved, hence it is sometimes termed “reaction rate theory.”

Both equations contain a defect production rate, which represents defects generated by radiation damage. The evaluation of this term is a challenge, as it is mainly a function of the material, the radiation field intensity, the radiation energy, the type of radiation and temperature.

Displacements, which are the source of point defects, are produced by elastic collisions between a moving particle and a static atom on its crystal lattice. If the energy transferred by the moving particle to the static particle is enough to remove from the lattice, then a displacement occurs. The moving particle could be the radiation particle or a knock-on atom (atoms belonging to the irradiated material which have been displaced and move with significant energy). This process continues until the radiation particle and the knock-on atoms come to a stop.

The calculation of the number of displacements produced per radiation particle requires the knowledge of the range of that particle (distance traveled from its creation or insertion into the material to the place where it stops). The stopping of the particle is caused by three different effects: (i) at high energy the particle (if charged) slows down through electronic ionization events, (ii) at lower energy the particle transfers (some of) its energy to other particles by colliding with them (elastic interaction) and, also, (iii) a fraction of the particle energy is lost by phonon emission (not explained here, but essentially

creation of vibrations in the surrounding material). The interaction of a charged particle with the electronic clouds of the material atoms, and which leads to their ionization, is responsible for part of the energy loss of the radiation particle, though without producing any considerable number of displacements. Once the energy of the particle is reduced down to a critical value, its own ionization level drops and it becomes essentially neutral, then the probability of the particle displacing an atom from its lattice increases and atom-atom collisions start happening. The energy transferred by the particle to the impacted atom depends on the energy of the particle, on the angle of collision and on the masses of both the particle and the atom. The energy transferred must be sufficient to break the bonds which keep the atom in its lattice place and, also, must be able to exceed a threshold energy level if it is not to return back to its original place. The atoms that are displaced by the particle are known as primary knock-on atoms (PKA). These PKA will keep on displacing other atoms until the residual kinetic energy is not enough to displace any additional atom.

In a first approximation to the quantification of the number of displacements, a simple approach was proposed by Kinchin and Pease [12]. Their theory provides the number of displacement per atom (dpa) produced by an incident particle. In the case of damage by fission fragments, the incident particle is a heavy ion of high energy. As each fission event yields two fission fragments, if one multiplies the dpa produced by each of them by twice the fission rate, one would obtain the point defect production rate. However, for several reasons, this approximation is not very accurate in the case of this study.

The first problem in using this approach is that the point defects, especially in the case of high energy heavy ions, are produced in a heterogeneous spatial distribution, while the rate theory generally used, which neglects the spatial gradient term, considers them to be homogeneously distributed within the material. Adding a corresponding descriptive term to the differential equations would imply increasing the complexity of the problem and, with that, solution times. Rather, the behavior can be approximated by assuming that a fraction of the produced point defects can freely diffuse into the bulk material while the balance of defects remain clustered in the zone of the damage cascade

Apart from this main limitation, the Kinchin and Pease model only considers the initial formation of displacements and ignores any annealing that may occur during the cascade event. During the collision cascade events large amounts of kinetic energy are lost over a short distance, heating the material to extremely high temperatures. This phenomenon used to be traditionally known as a thermal spike. Even though this peak in the temperature dissipates very quickly, a considerable fraction of the generated defects recombine during the spike event. Also, because of the clustering of defects and the consequent proximity of interstitial and vacancy clusters further annealing is expected, with a recombination rate above the one considered for the rest of the bulk material.

All these effects justify a reduction of the dpa per fission that is used in the production rate theory. The literature agrees that the freely migrating defects could be a mere 1% to 10% of the amount calculated by the K-P model.

Defect clustering and nucleation of clusters

The nature of collision cascades, in which atoms are displaced from a core volume and embedded into the surroundings of that core as interstitials, implies that the assumption of every displaced atom being equivalent to a created freely migrating vacancy/interstitial pair may be very simplistic. What several studies suggest is that vacancy and interstitial clusters are created, which are not free to move and diffuse to the bulk volume of the material. Moreover, some vacancies from the vacancy cluster recombine with interstitials in the interstitial cluster, diffusing only a short distance.

Also, the clusters play a major role in the generation of extended defects. Clusters tend to rearrange into more stable configurations. This is how interstitials form interstitial loops and vacancies form voids and vacancy loops. Such loops are disks of the corresponding elemental defect (2-D defects) which can grow, shrink and coalesce or annihilate with other loops. These loops are a type of mixed dislocation, thus may be termed "dislocation loops."

A look at the relevant literature indicates that clusters may nucleate into loops [13]. The rate at which such nucleation occurs is governed by the rate of increase or decrease in concentration and size of the clusters, which depend on the interaction between the clusters and nearby point defects. If the net flux of vacancies into an interstitial cluster is higher than the flux of interstitials into the same cluster, then the cluster would shrink and ultimately disappear; if the net flux of interstitials is higher, then the cluster would grow.

For the description of such a behavior, a model was developed as a rate theory that considers the influence of every cause of growth or shrinkage for each loop size [13, 14]. Assuming that the behavior is a consequence of fluctuations in point defects and cluster concentrations, the rate equations are reduced to a model that uses the Fokker-Plank equation, converting loop size (expressed as a number of defects – naturally an integer) into a continuous variable, even though it is actually a discrete variable. Through this treatment, it was possible to find a critical loop size above which loops continue to grow and below which they shrink. In this way, a probability for the cluster to nucleate, the most relevant feature of this model, is obtained. The most immediate conclusion of the Fokker-Planck-type models is that not all the clusters formed during the cascade events will evolve into loops. The nucleation probability will depend to a great extent on the maximum size a loop may attain before joining the dislocation network: the higher this value, the lower the probability [10, 13].

The size at which a loop would join the network can be determined using the stacking fault energy (see page 296 and Eq. 7.62, p 308 in [10]). Interstitial loops are faulted defects that are inserted between lattice planes, in the same way as precipitates would be. A defect is termed faulted because it introduces a discrepancy in the stacking sequence of crystallographic planes [15]. Such a stacking fault configuration is characterized by a particular intrinsic energy that is balanced by the surface energy of the material surrounding the loop. As the loop grows, there a point is reached at which the stacking fault energy is no longer enough to keep the surface energy of the material surrounding it. At that point the loop unfaults and becomes a perfect loop composed of edge and screw

dislocations. This new configuration, in contrast with the faulted loop that are sessile (immobile), is glissile (mobile) and can glide in its slip plane and move towards the dislocation network.

If one were to expand the model presented in this work to incorporate the concept of loop unfaulting, one would have to postulated that the Frank loop growth is limited by a critical loop diameter (or radius) at which said loop unfaults. This critical diameter is found by comparing (i.e., equating) the energy of a Frank loop, E_F,

$$E_F = \frac{2}{3}\frac{1}{1-\nu} G b_v^2 \frac{dr_I}{2} \ln\left(\frac{4r_I}{r_c} - 2\right) + \pi r_I^2 \gamma_{SFE}, \tag{3}$$

against the energy of a perfect loop, E_P,

$$E_P = \frac{2}{3}\frac{1}{1-\nu} + \frac{1}{3}\frac{2-\nu}{2(1-\nu)} G b_v^2 r_I \ln\left(\frac{4r_I}{r_c} - 2\right) \tag{4}$$

where r_I is the loop radius, ν is the Poisson Ratio, G is the shear modulus, b_v is the Burgers vector and r_c is the dislocation core radius.

Upon rearranging, the critical radius, r_{Ic}, is shown to satisfy

$$\gamma_{SFE} = \frac{1}{3}\frac{2-\nu}{2(1-\nu)}\frac{\mu b_v^2}{\pi r_I} \ln\left(\frac{4r_{Ic}}{r_c} - 2\right) \tag{5}$$

Or, equivalently, the Frank loop will unfault when it grows to a radius that satisfies the following inequality:

$$\gamma_{SFE} > \frac{1}{3}\frac{2-\nu}{2(1-\nu)}\frac{\mu b_v^2}{\pi r_I} \ln\left(\frac{4r_{Ic}}{r_c} - 2\right) \tag{6}$$

This concept of loop unfaulting is not included in the main model developed in this work. Instead, loops and straight dislocations that are not part of the network will be considered as a single species and assumed to be glissile. However, the concept of unfaulting will be revisited in the Appendix IV.

From this section it can be concluded that it is important to include the concept of clustering in the model for two reasons: (i) not to calculate an excessively large number of point defects released to the bulk of the irradiated material and (ii) to estimate the number of interstitial loops that nucleate from interstitial clusters.

The interstitial loops constitute the main source of dislocations that can get captured by, and feed the growth of, dislocation networks. In the opposite direction, dislocation networks act as sinks for interstitial clusters in which interstitial loops are primarily formed. These competing effects lead to the conclusion that a saturation density of dislocation networks can be hypothesized.

A critical density for dislocation networks and, consequently, a critical subgrain diameter, can be proposed for which the strength of sinks acting over clusters is too high to allow them to nucleate into new interstitial loops.

Experimental support for this theory is difficult to find, mainly because it is not easy to get accurate measurements of dislocation density for high densities. Thus, the idea that the dislocation density reaches a saturation value is proposed in the literature [16] without complete confidence. However, it will be assumed that the aforementioned value exists and has an observable effect in the model.

Recovery and recrystallization

Two important phenomena must be introduced to understand the developments shown in this work: recovery and recrystallization. These phenomena are usually observed during annealing of cold-worked materials. Stresses applied to materials during cold-work produce dislocations and/or increase their concentration. The produced dislocations confer upon the material some mechanical properties that may not be desired, so the worked piece is usually subjected to a thermal treatment [17, 18]. During such thermal treatment, dislocations experience increased mobility; this effect promotes their migration, and growth, as well as the recombination of opposite dislocations and possible reordering into more stable arrangements. Sometimes ambiguously called polygonization, recovery ultimately arranges the dislocations into cellular dislocation networks. The size of these networks (i.e., its diameter) is given by an energy balance where dislocations, taking a cellular arrangement, lower the stored energy. This theory will be fully developed in Appendix II.

Once the material is subdivided into subgrains by the dislocation networks, another process can occur, which is named recrystallization. Multiple explanations are proposed for explaining recrystallization, and perhaps most of them are correct depending on the prevailing physical conditions. However there still is no unifying theory on how grains recrystallize.

Recrystallization theories have in common the tendency for the subdivided material to reduce its stored energy, which is concentrated in dislocations, by reducing its grain size

and increasing the presence of grain boundaries or rather increasing the overall area of grain boundaries per unit volume. Of course, the increase of grain boundary has a cost in energy, which is met by energy supplied from the stored energy. How the stored energy is transferred to the newly created grain boundary seems to be the main discrepancy between theories.

Nevertheless and irrespective of their differences, the theories all have in common a similar mechanism that governs the process of formation of recrystallized grains through the formation of a new grain from several subgrains, as they coalescence or are absorbed into the new growing grain.

A special case of recrystallization is observed when the material is deformed at high temperatures, namely dynamic recrystallization. During dynamic recrystallization, the dislocation generation, recovery and recrystallization steps occur simultaneously. As the fuel pellet will be at moderate to high temperatures in the I^2S case, it is expected that this mechanism would be one to consider in this work.

It can be found in the literature that various types of radiation have an enhancing effect on recrystallization. The creation and growth of subgrains dividing grains has been observed in irradiated copper. These measurements conclude that radiation accelerates recrystallization when compared to normal (i.e., ordinary) cold-worked copper grain refinement [19]. A similar effect is postulated for nuclear fuels, with the difference that in these the dislocations are not generated by the effect of external stress, but by radiation damage.

As can be seen later in this work, in the model proposed for grain subdivision, a critical recrystallization burnup or fission density has to be estimated and, for this, an energy balance is used, in which the stored energy is consumed for the creation of the new grain boundary.

Number of recrystallizing atoms: creep effect

It is proposed that the transition between grains divided into subgrains to new recrystallized grains occurs due to a rearrangement of the sub-boundaries, composed by dislocations, which make the subgrains coalesce or rotate to cancel the misorientation angle with adjacent subgrains while increasing the misorientation of the cluster of subgrains that will form the new grain with the rest of the surrounding material.

A similar effect is postulated for nuclear fuels, with the difference that in these the dislocations are not generated by the effect of external stress, but by radiation damage.

$$n_{subgr} = C\sigma^n e^{-\frac{Q_{creep}}{kT}} \tag{7}$$

where C, n and Q_{creep} depend on the material. As can be seen in this equation, it is a process activated by stress and temperature. It can be furtherly assumed that the stress is proportional to the dislocation density, yielding the following expression:

$$n_{subgr} = C'(b_v^2\rho_N)^n e^{-\frac{Q_{creep}}{kT}} \tag{8}$$

It may be presumed from this expression that, at low temperatures, subgrain mobility would not be high enough to promote recrystallization. Another physical conclusion from

this equation is not as straightforward to see and pertains to high temperature behavior. Under high temperature conditions the Arrhenius term is significantly larger and could suggest a higher number of subgrains being formed. However, at high temperature, recovery is enhanced. This means that the network dislocation density decreases, which also implies a decrease in stress. These changes imply that the power term decreases. Then, the power term and the exponential term will compete with each other, possibly resulting in a critical temperature at which n_{subgr} will reach a maximum.

CHAPTER 3

Swelling

One of the most important physical changes to take into account when designing a fuel element is swelling and correspondingly, one of the most important parameters is the swelling rate. Fuel pellets will go through a buildup of different dimensional changes during their lifetime in the reactor. One of them is swelling which accumulates with burnup. The other effects affecting the pellet's size are densification, which reduces the as-fabricated porosity during the first days of irradiation, and thermal expansion.

Swelling of nuclear fuels can be caused by two different drivers: gaseous fission products and solid fission products. Solid fission products in solution within the fuel matrix cause a distortion of the crystalline network. This distortion increases the separation between the equilibrium sites of the crystal, resulting in a macroscopic increase of the size. On the other hand, gaseous (and volatile) fission fragments aggregate into bubbles of different sizes; therefore, each of these needs a different treatment. It should be added that isolated gas atoms have a similar behavior as that of the solid fission fragments.

This work focusses on the swelling caused by the gaseous fission fragments. It is an attempt to identify the key variables and parameters that affect swelling and to obtain a comprehensive model that predicts grain subdivision, as grain size has a mayor effect on the final result. Grain subdivision has been related to an increase of the swelling rate observed as a "knee" in plots of swelling versus fission density, as described later.

Swelling due to solid fission fragments

Accumulation of solid fission fragments produces swelling in irradiated nuclear fuels as these atoms perturb the crystalline structure of the fuel material. The presence of these foreign atoms is known to cause an increase in the volume of the fuel. Expression for the contribution of solid fission fragments are already known for UO_2 and will be extracted from literature without further considerations [20].

Swelling due to gaseous fission fragments

Swelling of materials under irradiation has been largely studied since the early stages of nuclear energy [1, 21, 22]. Not only has there been interest in swelling affecting nuclear fuels, but also in swelling affecting structural materials, reducing their lifetime through to radiation damage [10]. Still there are differences in the analysis according to the component, as the temperature and the radiation flux, energy and type are completely unalike. However, the swelling of structural materials, mainly generated by neutron damage, has points in common with the swelling of nuclear fuels. In both, cavities are generated within the material. These are voids in the case of structural materials and bubbles in the case of nuclear fuels. The difference resides in that fission products are generated with each fission event and a fraction of them are gases. These gas atoms cluster, forming bubbles. On the other hand, voids in structural materials are made from clusters of vacancies.

Bubbles still need vacancies to form the cavity, therefore bubbles can be in equilibrium or overpressurized, depending on whether there are enough vacancies present for the original cavity to be as large as the gas atoms collected inside require. The equilibrium radius of the bubbles can be obtained using a gas Equation of State (e.g., Van der Waals gas equation) and balancing the pressure with the surface tension of the fuel.

Olander [22] describes in a simple way why the grouping of gas atoms in larger bubbles evolves into a larger swelling through the following reasoning. Using Van der Vaal equation of state, the number of a gas atoms m in a bubble of radius R, is given by:

$$\mathrm{m} = \frac{4\pi R^3}{3\left[B + \left(\frac{kT}{2\gamma}\right) R\right]} \tag{9}$$

where T is the temperature, k is the Boltzmann's constant, γ is the surface tension and B is the Van der Vaals constant.

For small bubbles (R < 10 Å) and for large bubbles (R > 1000 Å), limiting cases can be found (equations (10) and (11), respectively).

$$\mathrm{m} = \frac{4\pi R^3}{3B} \tag{10}$$

$$\mathrm{m} = \frac{4\pi R^2}{3\frac{kT}{2\gamma}} \tag{11}$$

If the swelling in a section of the fuel ($\Delta \mathrm{V}/\mathrm{V}$), assuming that all the bubbles have the same size, is given by:

$$\Delta V/V = N\frac{4}{3}\pi R^3 \tag{12}$$

where N is the number of bubbles in the volume V. Then, if the N bubbles coalesce into $N/2$ bubbles, the change in the swelling will be given by

$$\frac{(\Delta V/V)_f}{(\Delta V/V)_i} = \frac{R_f^3}{R_i^3}\frac{N/2}{N} \tag{13}$$

If after coalescing, each bubble has double the number of gas atoms, it can be concluded that

$$\frac{(\Delta V/V)_f}{(\Delta V/V)_i} = 2^p\,\frac{1}{2} \tag{14}$$

where p will take different values for different bubble radii. From the limiting cases, one can infer $p = 1$ for small bubbles and $p = \frac{3}{2}$ for large bubbles. Therefore, the effect of bubble coalescence on swelling increases with increasing bubble size, being null for bubbles formed by only a few gas atoms.

Due to radiation re-solution, the size of the intragranular bubbles can increase merely to the limit of the small bubbles; however if bubbles grow at grain boundaries, their size can be significantly larger. Then, if gas atoms migrate to grain boundaries and join existing bubbles, swelling would increase. This explains the importance of the grain size for swelling rate calculations and, consequently, of determining if grains subdivide under irradiation, when would this happen, and what would be the resulting grain size. Without further analysis detail, this is the basis of gaseous fission product swelling. A proper

swelling calculation should include a comprehensive analysis of every effect playing a role in the bubble behavior. Also, a distribution of bubble sizes will exist and it must be evaluated. In the end, the volume of all the bubbles (and cavities) generated in the irradiated materials is summed up to get the amount of volume increase.

Actual models

Several theories and models have been proposed to explain the swelling of nuclear fuels in a way that fits available experimental data. MATPRO [20] includes a well-accepted model for calculating the swelling due to solid fission fragments and that model is the one considered in this work. Less agreement is reached for the swelling due to gaseous fission fragments. Different codes were developed to calculate the swelling in fuels using a mechanistic analysis of the nucleation, growth and migration of bubbles (i.e. GRASS-SST [23], FASTGRASS [24], DART[25]). These codes also link the swelling behavior to fission gas release, which from the vantage point of the material under irradiation constitutes a sink for the gas generated during fission.

Even when it can be thought that the gas fission fragment mechanism of swelling has been understood and quantified, there still remains an unresolved issue. A required input of the codes that model swelling is the crystalline grain size. Indeed, volatile species and intragranular bubbles can migrate to grain surfaces, edges and nodes. These sites are more stable and they favor coalescence of the bubbles, therefore modifying the final result of swelling calculations, sometimes by orders of magnitude.

The above considerations should make it obvious that a model that predicts the grain subdivision of fuels with good accuracy is very important. Grain size reduction, which with some degree of bias has been called grain subdivision before, can be caused by different mechanisms. The most accepted mechanism for this to happen is the recovery and recrystallization [1, 16, 26-29]. Through this mechanism, dislocations generated during irradiation group together in networks enclosing volumes of materials containing a relatively low dislocation density. These volumes are called subgrains and are the nuclei of future recrystallized grains, with a size orders of magnitude lower that of the as-fabricated grain size. However, it has not been completely proved that this is the actual mechanism. Other theories propose that grain size reduction can be caused by stress-induced cracking or due to overpressure in bubbles.

One more statement must be made, particularly in the case of U_3Si_2 under irradiation. It was proposed that swelling can occur after the material has been amorphized by radiation damage [30-32]. If this happens, bubbles nucleate and grow in a liquid-like matrix [31, 32]. This work proposed that this situation is plausible only in low temperature irradiations, far from the temperature at which the fuel will be in a power reactor such as the I^2S-LWR.

The "knee"

Both grain subdivision and bulk amorphization offer an explanation to the change in swelling rate (dubbed the "knee") reported by experimentalists [1, 31, 32]. As it can be

surmised, if grains subdivide, more grain boundary will form, producing larger areas of stable sites for bubbles to form and grow, thus enhancing swelling. If fuel undergoes amorphization, bubbles grow without being constrained by a crystalline structure, until a point at which bubbles start touching and coalescing. It is proposed that from the onset of that behavior the swelling rate will be higher.

CHAPTER 4

Models

Current swelling models for U_3Si_2 are focused on research reactors fuels, but new requirements emerge as advanced fuels are being designed for power reactors. I^2S-LWR includes the use of U_3Si_2 pellets as fuel in its preliminary design and hence needs a better model of the swelling than the already existing ones. In meeting this need, already existing models were modified and used.

The main model that serves as a starting point for this work is the one presented by Rest multiple times [1, 28, 31], but with some of his assumptions relaxed to obtain a solution scheme that is, nowadays, possible to implement due to improvements in computational capacity and speed that allow efficient and effective solutions using complex computer codes. Apart from this, some new assumptions are made that are different from the ones in the previous work by Rest.

Rest postulates a swelling model where bubbles within the bulk region of a crystal are prone to undergo re-solution under irradiation, but on the other hand if bubbles diffuse to the grain boundaries, they would find a more stable place to coalesce and grow. Therefore, it is highly important to know the evolution of grain size and, as a consequence of this, the average distance to grain boundaries. Hence, Rest introduced a model for predicting grain subdivision (and the consequent creation of grain boundaries).

Another approach for the U_3Si_2 swelling was introduced in a paper presented in ICAPP 2014 and used in the BISON code [33]. The model used for swelling in that publication is an empirical expression obtained from data presented in Finlay's paper on "Irradiation behavior of uranium silicide compounds" [34]. The first comment that can be made about this approach is that it considers swelling of fuel particles in mini-plates at low temperature, where a different swelling mechanism is expected to prevail compared to the mechanisms in U_3Si_2 at power reactor conditions (see next section). This expression, not only ignores temperature effects in swelling, but also ignores the fact that the fission rate affects swelling, which is mentioned in that same paper. Moreover, strain values shown on the referred-to paper belong to samples with geometry completely different from that of pellets.

The expression used together with the BISON code can be extensively improved upon through detailed representation of microstructure evolution under irradiation, gas migration and material strain. Then, swelling should be pondered throughout the pellet volume by averaging contribution of microscopic swelling into total macroscopic strain. These considerations would lead to a more complex correlation between the various underlying parameters of swelling, which results in the ability for predicting swelling under a wider range of conditions.

In their approach, the BISON model authors also consider densification of the fuel in the reactor. This effect is merely extrapolated from UO_2 behavior, despite the very different nature of U_3Si_2 compared to UO_2.

The use of extrapolated data from UO_2 and the assumption of some similarity of performance could be construed as legitimate in view of some (limited) similarities in material morphology. Indeed, it can be expected that if pellets are manufactured through pressing and sintering, some remaining porosity will exist in the pellet and, due to temperature effect and radiation enhanced diffusion, some densification could be observed. If the pellets are manufactured by casting, then less porosity would be expected. Densification in residence within the reactor can be predicted through modeling or it can be considered an input parameter if this can be inferred from and correlated with the fabrication process (i.e. an acceptable pellet morphology must exhibit less than a determinate percentage of densification after some specific test.)

The Standard ISO 15646:2014 [35] describes the procedure for measuring the densification of some Uranium oxide compound pellets. It states that densification will depend on pore size, spatial pore distribution and grain size.

Amorphization vs. grain subdivision

Regarding the choice and validity of swelling models for U_3Si_2, there exists in the literature a dichotomy that must be explained. There are two competing theories: (i) one that postulates a mechanism dominated by grain subdivision and (ii) one that assumes amorphization and subsequent evolution. Both theories attempt to explain the bubble behavior in the fuel and both also propose an explanation for the "knee" in the swelling rate.

The amorphization model states that radiation damage generated in the material turns it from a crystalline to an amorphous phase. When this happens, a different approach must be used from the one used if the material remains crystalline.

Experiments provide proof that the U_3Si_2 material becomes amorphous at relatively low levels of radiation damage [31]. However, these experiments were performed at low temperature, where defect migration is very slow. So, under such a condition, annealing of the material is not probable and clusters of damaged material start accumulating. If radiation applied to the material for some time, there will be a point at which the fraction of damaged material is high enough to consider the material amorphous.

Yet, this scenario is modified when the temperature goes up. As temperature becomes higher, defects mobility increases, allowing the material to recover its crystalline structure after each damage event. A critical temperature is considered to exist, at which there is no dose that could amorphize the material. Literature establishes that temperature for U_3Si_2 at around 450 K [31] (see Figure 1). If this value is considered reliable, then amorphization is virtually impossible under power reactor conditions.

On the other hand, if the fuel temperature during irradiation exceeds the amorphization critical temperature, damage starts taking the form of an increase in the concentration of point and extended defects within a persisting crystalline structure. This line of thinking was proposed for U_3Si_2 [1], but then abandoned and replaced by the amorphization theory as models were created for U_3Si_2 performance under research reactors conditions, in which the temperature is lower than the amorphization critical temperature. However,

evidence was subsequently found that, in ion-irradiated U_3Si_2, grains went through subdivision when irradiated at temperatures higher than the critical temperature [36]. Fortunately, the initial line of thinking, now supported by this latter evidence, remained under development by several authors [27, 28, 37-41] as a valid theory to explain the rim effect observed in high burnup structures of UO_2 fuels.

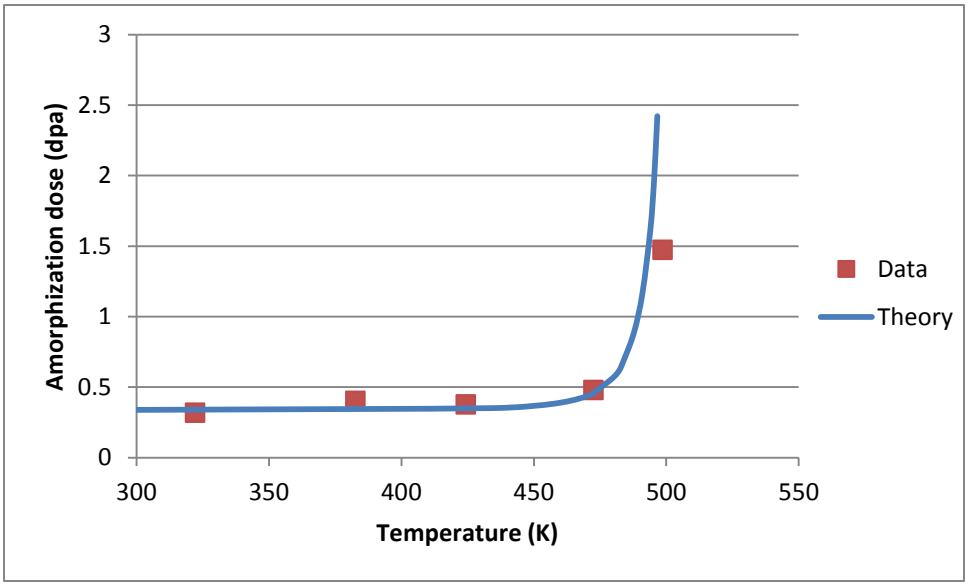

Figure 1. Temperature dependence of dose required to amorphize U_3Si_2 after [31].

Rim effect

The name rim effect is assigned to the structure seen in the periphery of UO_2 pellets, especially at high burnup levels. For this reason it is also known as high burnup structures. It consists on a porous section of the pellet caused by a reduction of the grain size and an increase in the concentration of bubbles. Its occurrence is attributed to the

lower temperature and higher fission rate and fission density at that rim. As burnup increases, the thickness of the rim is observed to increase. The formation of this structure has considerable effect on the fission gas release behavior, the thermal conductivity and the swelling behavior. As the effect that this structure can have on fuel performance may be substantial, some efforts have been expended to predict when and how the rim will appear. These models resemble the ones previously postulated for grain subdivision in U_3Si_2, but subsequently abandoned in favor of the amorphization theory. However, modeling of grain subdivision leading to the rim effect has been developed more in depth, as it is considered the best existing explanation for that latter phenomenon.

This work develops a new model based on the grain subdivision concept and specializes it for application to U_3Si_2. The new model is now applied to temperatures above the critical amorphization temperature, where its validity can be claimed. It must be understood that the main objective of modeling the rim effect in UO_2 is to relate it to fission gas release, as its thickness is negligible compared to the radius of the pellet, minimizing its influence in the swelling. In contrast, the thickness of the high burnup structure in U_3Si_2 can be larger than the one observed in UO_2, thus it could have a considerable effect on the swelling performance. It is this performance that the model in this work attempts to determine and quantify.

Experimental observation on the rim effect

Apart from the experimental data available for swelling in U_3Si_2, it is important to acknowledge the data available on grain subdivision in UO_2 as it is important for the model developed in this thesis. Research on grain subdivision has been carried out by several authors for a long time due to its effect on thermal conductivity and gas release of the pellets.

The interest in those experimental data for the present work has a different motivation, namely the validation of the new model prior to extrapolating it to U_3Si_2. This would subsequently allow the prediction of the effect of grain subdivision on swelling.

Early papers on the rim effect pointed out the presence of a porous band in the periphery of the pellet of LWR reactors [42]. From the concentration of Pu, it was possible to recognize an increase in the burnup towards that region. This led to the conclusion that a combination of low temperature and high fission rate was responsible for this phenomenon.

Another set of authors observed a reduction in the grain size in the rim and a decrease of the concentration of Xe expected when compared with other fission products [43]. This depletion of the Xe content was, however, considering only lattice Xe, therefore it did not included the Xe present in large pores. An increase of the rim thickness with increasing burnup was also observed.

Some authors started pointing out the presence of dislocations near the restructured region [43, 44] and propose that they may play an important role in the definition of the new structure.

Thomas et al. [44] clarified the definition of rim effect which was ambiguous at the time and redefined it as the region were the fuel goes through grain restructuring, differentiating it from the definition of rim as the region where the absorption of epithermal neutrons generates Pu and displays a high the fission density and beyond which Pu generation and fission density drop drastically due to self-shielding. A local burnup threshold was found to be around 70-80 MWd/kgM and the upper temperature limit around 1100°C.

Une et al. [45] recognized the importance of the formation of dislocation networks in the restructuring of the fuel material. Ray et al. [46] published a paper with transmission electron microscopy images showing the grouping of dislocations in irradiated fuels. Nogita and Une [16, 40] continued investigating the role of dislocation density increase with burnup on grain subdivision. They observed the formation of extremely tangled dislocations forming low angle boundaries. They recognized the presence of subgrains of 20 to 30 nm average diameter and recrystallized grains from 50 to 200 nm in size.

CHAPTER 5

Grain subdivision Model

In the previous chapters a summary of the information from the literature was presented that support the hypothesis of grain subdivision as a mechanism underlying swelling in crystalline materials at high temperature. The search of the literature and the description of the mechanisms set the stage for the development proper of a grain subdivision model. This development can now be presented. The new model is a modification of Rest's model, which has been explained in the previous chapters.

Several assumptions made in the original model describing the evolution of the microstructure in the material were relaxed as they were not completely valid for the cases that are studied in this work. Furthermore, the way in which the critical dose for subdivision is attained has been changed. It was found that, for Rest's critical dose calculations to be valid, the system had to reach steady state, however this was not the case in part of the temperature range under study. Moreover, the steady state values used in the model are valid for very simplified systems, but in the case of fuel undergoing irradiation inside a reactor, the microstructure would evolve into very complex systems that would require a more complex solution. As grains subdivide under conditions away from the simplified situation of Rest's models, it has been concluded that a new way of finding the critical point had to be worked out to replace the older original one.

Critical dose

The novel concept introduced in this work towards the modeling of grain subdivision is the calculation of the critical dose (i.e., dose at which a grain subdivides). Rest obtains this value through an energy balance that equalizes the stored energy due to deformation and the surface energy of a hypothetical new grain, leading to a critical grain diameter. As the stored energy increases, the recrystallized grain size decreases. It is stated in Rest's development that dislocation network density reaches an equilibrium stage rather fast during irradiation and, hence, steady state values are obtained for the microstructural composition. Working out his equations, an expression is obtained where the critical fission density can be approximated by a Boltzmann equation based on solute recrystallization theories. Finally, Rest obtains an "activation energy" for the grain subdivision process.

This work, although using a similar basis, proposes that recrystallization occurs during a transient (non steady-state) evolution. This modification is proposed for two reasons: the time to achieve steady-state at low temperature may be high and the sink concentration is high and changes in time. Rest approximates the point defect concentrations with the equilibrium concentration from equations (15) and (16), obtained after Sizmann [11].

$$\mathrm{C_v^{eq}} = \sqrt{\frac{Q_0 K_{is}}{K_{iv} K_{vs}}} \tag{15}$$

$$\mathrm{C_i^{eq}} = \sqrt{\frac{Q_0 K_{vs}}{K_{iv} K_{is}}} \tag{16}$$

In equations (15) and (16), Q_0 stands for the rate of point defects production, K_{iv} is the recombination rate, K_{vs} is the rate at which vacancies react with sinks and K_{is} is the rate at which interstitials react with sinks. The equilibrium values obtained through these equations are only valid for low temperature and a low sink concentration. The problems with using them are, on one hand, that the sink concentration will be high because of the high dislocation density and, on the other hand, the time needed at low temperature to reach the equilibrium is high.

As it is proposed that recrystallization occurs during a non-equilibrium state, the hypothesis of approximating the critical fission density through a Boltzmann equation becomes invalid and is dropped. Therefore, another condition must be developed for finding the critical values. To find a plausible answer for this, we refer to the better known recrystallization processes in cold-worked metals.

Recrystallization, or grain refinement as it is sometimes called, in cold-worked metals have been thoroughly studied. It is the process by which highly deformed (high dislocation density) pieces are heated to promote the reorganization of dislocations into new grain boundaries, leading to smaller grains. This process has several applications in the industry due to the huge change in the mechanical properties of the treated piece.

As has already been explained, to decrease the stored energy of the dislocations, they (the dislocations) rearrange in cellular structures delineating or forming subgrains.. These subgrains are the nucleus for the recrystallization process. When thermal processes are activated at elevated temperature, subgrains coalesce to form a recrystallized grain. For

this reason, another difference with Rest's model is introduced: Rest calculates a recrystallized grain size smaller than the subgrain diameter, which might only be possible if grains nucleate at the triple junctions of the dislocation network, but the grain and subgrain sizes should at least be equal. However, if the grains recrystallize due to the coalescence of subgrains, the new grain size **must** be larger than the subgrain diameter.

This work proposes that there is a link between the coalescence of grains, where dislocation networks must travel in "packets" to other cell walls, and creep. Then, the distance travelled by those "packets" may be dictated by a formula similar to the steady state creep with an activation energy and a dependence on stress in the pre-exponential factor. It can be concluded from this analogy that the amount of subgrains recrystallizing into one grain will be proportional to that distance.

In a way, following a strict mathematical formulation and formalism, the new developments are not a completely dissimilar with Rest's solution, as the creep formula used is similar to the Boltzmann equation. The difference is that while Rest fits the Boltzmann equation to a curve for a steady-state concentration of interstitial loops, in the present work the recrystallization is obtained through the crossing of two curves that evolve in time.

The following logical step is to obtain the critical values. To do so, the recrystallized grain size must be set equal to the subgrain diameter multiplied by the cubic root of the number of subgrains that coalesce to form the new grain. As deformation, and therefore dislocation density, increases, the recrystallized grain size decreases. If at any moment

the size of the recrystallized grain is actually equal to the subgrain size multiplied by the cubic root of the amount of subgrains coalescing, the subgrains are considered to have enough energy to recrystallize into a new grain. If the two calculated diameters are never the same, the grain will not recrystallize.

It must be understood that this work does not claim that this method to obtain the critical dose represents the whole reality of the physical situation, as several complex microstructural changes happen simultaneously. However, the method is considered a good assumption that makes it possible to easily predict the recrystallization point while taking into consideration the thermal and stress effects in the coalescence process intensity.

Microstructural evolution

The modeling of the microstructural evolution developed in this work is based on the model used by Rest in his work. However, several modifications have been introduced in an attempt to increase the fidelity of the model. Apart from this, a transient solution is obtained using a computational ODE system solver, as it is recognized that the steady state is not always achieved before recrystallization occurs.

In the original model, a significant ambiguity exists on the definition of a characteristic diameter. That model represents indistinctly dislocation loops of any size and dislocation network diameters, sizes that may differ by orders of magnitude. A concept introduced by Rest in [47], but which was not fully developed, is adopted; but the present model

development work adds a differential equation for quantitatively characterizing the evolution of the average loop diameter. This is incorporated into the model independently from similar considerations on the dislocation network cell diameter. This new model considers that equation in order to be able to calculate separate diameters.

Also, a "new" species is included: the di-interstitial loop. It is used as a buffer species; di-interstitials can be destroyed into single interstitials or can grow, but once they grow they cannot be reduced back to di-interstitials. They also differ from larger interstitial loops in that they can be created directly in a radiation damage event and/or from the clusters formed by cascades. Di-interstitials have a fixed diameter equivalent to two atomic distances.

Even more accurate results may be obtained if more loop species are added. A loop species would depend on the amount of interstitials that constitute said loop, in average, within a certain range. However, the inclusion of each one of the species would add two differential equations to the model, one for the concentration of that particular-sized loop and another one for its characteristic diameter, which varies as it is an average value. A "perfect" description may be reached if every loop size is considered; in this case the diameter equations would not be necessary as every species would have a defined diameter, but, on the other hand, the number of equations added for the concentration of each of the loop sizes would be extremely high, increasing convergence time of the solver.

Equations for microstructural evolution

The two possible point defects that can normally exist in a microstructure are vacancies and interstitials (although impurities added during irradiation are also point defects), which have thermal equilibrium concentrations, but these concentrations generally experience increases due to collision cascades during irradiation. During cascade formation events, atoms are displaced from their lattice sites and pairs of interstitials and vacancies are generated. These defects would recombine or annihilate at a certain rate. From the balance of generation and consumption (including recombination), an equilibrium concentration may be found, as described by the following two equations:

$$\frac{dC_v}{dt} = Q_v - K_{iv}C_vC_i - K_{vN}(\rho_N)D_vC_v - K_{vL}(\pi C_I d_I)D_vC_v - k_{gb}^2 D_vC_v - \frac{4\pi a_0^2 D_v C_v C_{2i}}{\Omega} \tag{17}$$

$$\frac{dC_i}{dt} = Q_i - K_{iv}C_vC_i - K_{iN}(\rho_N)D_iC_i - K_{iL}(\pi C_I d_I)D_iC_i - k_{gb}^2 D_iC_i - 16\pi r_{iv}D_iC_i^2 + \frac{4\pi a_0^2 D_v C_v C_{2i}}{\Omega} \tag{18}$$

Eq. (17) represents the balance of vacancies concentration where the contribution of the vacancies generation, the recombination with interstitials and the annihilation to network dislocations, loops, grain boundaries and di-interstitials are considered, respectively. Eq. (18) represents the balance of interstitials in which are considered the generation, the recombination with vacancies, the annihilation to network dislocations, loops and grain boundaries, the loss due to formation of di-interstitials and the creation due to reaction of vacancies with di-interstitials [1, 27, 48].

The point defect generation rates are given by:

$$\mathrm{Q_v} = \mathrm{Q_i} = \frac{\dot{\mathrm{f}}}{B} \tag{19}$$

The respective diffusion coefficients are calculated as follows:

$$\mathrm{D_v} = \mathrm{a_0^2 \nu_0^v} e^{-\frac{\epsilon_v^m}{k_b T}} \tag{20}$$

$$\mathrm{D_i} = \frac{2}{3}\mathrm{a_0^2 \nu_0^i} e^{-\frac{\epsilon_i^m}{k_b T}} \tag{21}$$

where a_0 is the lattice parameter, ν_0^v, ϵ_v^m, ν_0^i and ϵ_i^m are the jump frequencies and migration activation energies for vacancies and interstitials.

The recombination rate and the grain boundary sink strength are given by:

$$K_{iv} = 40\pi r_{iv} D_i \tag{22}$$

$$k_{gb}^2 = \frac{24}{{d_g}^2} \tag{23}$$

where r_{iv} is the recombination radius between vacancies and interstitials and d_g is the grain diameter.

K_{jX} is the sink strength of dislocations which can be rewritten as:

$$K_{jX} = Z_{jX}\rho_X \tag{24}$$

with $j = i, v$ and $j = N, L$, indicating interstitials and vacancies and network dislocations and loops, respectively. The effect of the different value taken by this parameter for each

point defect is named dislocation bias, because of the higher tendency for interstitials to interact with dislocations.

Values for Z_{jL} and Z_{jN} are calculated according to Dubinko et al. [49]. This is done per

$$Z_{jX} = Z_{j0} + 2\sum_{n=1}^{\infty}(-1)^n Z_{jn} \approx Z_{j0} - 2Z_{j1} \tag{25}$$

with

$$Z_{jn} = \frac{2\pi I_n\left(\frac{L_j}{2r_0}\right) I_n\left(\frac{L_j}{2R}\right)}{I_n\left(\frac{L_j}{2r_0}\right) K_n\left(\frac{L_j}{2R}\right) - K_n\left(\frac{L_j}{2r_0}\right) I_n\left(\frac{L_j}{2R}\right)} \tag{26}$$

where I_n and K_n stand for the modified Bessel functions of order n, $R = \frac{1}{\sqrt{\pi\rho_D}}$, r_0 is the core radius of the dislocations, ρ_D is the total dislocation density and

$$L_{v,i} = \left|\frac{1}{3\pi}\frac{(1+\nu)Gb_v\Delta V_{v,i}}{(1-\nu)k_bT}\right| \tag{27}$$

where $k_b$is Boltzmann's constant, G is the shear modulus, ν is Poisson's ratio and $\Delta V_{v,i}$ stands for the relaxation volume of vacancies and interstitials, respectively.

As it can be seen, the concentration (or density) of other extended defects, like di-interstitials (C_{2i}) and dislocation networks (ρ_N), are required to solve equations (17) and (18) so it is necessary to include equations for them:

$$\frac{d\rho_N}{dt} = f_1\frac{|\nu_D|}{d_N}\pi d_I C_I - f_2\frac{|\nu_N|}{d_N}\rho_N \tag{28}$$

$$\frac{dC_{2i}}{dt} = Q_{2i} + 8\pi \frac{r_{iv} D_i C_i^2}{\Omega^2} - 4\pi \frac{r_{iv} D_i C_v C_{2i}}{\Omega} - \frac{\pi \nu_{2i} c_{2i}}{b_v} \quad (29)$$

Equations (28) and (29) are the balances for the dislocation network density and di-interstitial (and clusters) concentration, respectively. In these, ν_I stands for the dislocation climb, which is considered the limiting mobility mechanism for dislocations [37]. Dislocation networks are generated by dislocations as they develop into loops that join the network, whereas they are annihilated by recombination with an opposite dislocation due to recovery in the network. Di-interstitials are generated in collision cascades and by combination of two interstitials, destroyed by reaction with a vacancy. They can also grow into interstitial loops by climb.

In equation (28) and (29), f_1 and f_2 are geometric factors that have not been properly modeled in this work and will be estimated following the approach of Sandstrom [50].

The intermediary structure between defects generated directly by radiation and dislocations arranging into cell walls are the interstitial loops. Special attention is paid to them as they do not behave similarly to the other species. Loops are characterized by an average concentration and by an average loop diameter.

Then, the loop concentration (C_I) and its average diameter (d_I) are calculated by solving the following equations:

$$\frac{dC_I}{dt} = \frac{\pi \nu_I C_{2i}}{2a_0} - \frac{4\nu_I C_I d_I}{P_{sl}\, d_N^2} - 8\nu_I d_I^2 C_I^2 - f_1 \frac{|\nu_D|}{d_N} C_I \quad (30)$$

$$\frac{d(d_I)}{dt} = \nu_I - (d_I - 2a_0)\frac{\dot{C_{2i\to I}}}{C_I} - (d_N - d_I)\frac{\dot{C_{I\to N}}}{C_I} - d_I\frac{\dot{C_{2I\to I_2}}}{C_I} \quad (31)$$

$$\dot{C_{2i\to I}} = \frac{\pi\nu_{2i}c_{2i}}{2a_0} \quad (32)$$

$$\dot{C_{I\to N}} = \frac{4\nu_I C_I d_I}{P_{sl}\, d_N^2} \quad (33)$$

$$\dot{C_{2I\to I_2}} = 8\nu_I d_I^2 C_I^2 \quad (34)$$

The first term on the RHS of equation (31) stands for the change in diameter of the loops due to climb (growth or shrinkage according to the sign). From the second to the last, the terms are changes in the average diameter due to the growth of clusters into loops, the growth of loops into the network, and the coalescence of loops, respectively. The terms are arrived at using the following reasoning. The average diameter can be calculated at any time as

$$d_I = \frac{1}{n}\sum_i d_{Ii} \quad (35)$$

where d_{Ii} are the diameters of the n loops averaged. Then, the change in the average diameter between two instants, assuming the same amount of interstitials is present can be written as

$$\Delta d_I = d_I^f - d_I^0 = \frac{1}{n}\sum_i (d_{Ii}^f - d_{Ii}^0) \quad (36)$$

If only a small fraction of the population j ($j \ll i$) is added/removed from the population, then

$$\Delta d_I = \frac{1}{n \pm j} \sum_j (d_{Ij}^f - d_{Ij}^0) \approx \frac{1}{n} \sum_j \left(d_{Ij}^f - d_{Ij}^0\right) = \frac{1}{n} \Delta n_j \Delta d_j \tag{37}$$

and dividing by Δt

$$\frac{\Delta d_I}{\Delta t} \approx \frac{1}{n} \frac{\Delta n_j}{\Delta t} \Delta d_j \tag{38}$$

Multiplying and dividing the right-hand side by the volume and letting $\Delta t \to 0$, one obtains

$$\frac{\mathrm{d}(d_I)}{\mathrm{d}t} \approx \frac{1}{C_I} \dot{\mathrm{C}}_{\mathrm{Ij}} \Delta d_j \tag{39}$$

Here, as the initial or final loop does not exist depending on the case (whether a new loop is being formed or a loop transforms into another species), Δd_j is taken relative to the average diameter. $\dot{\mathrm{C}}_{\mathrm{Ij}}$ is the rate at which loop concentration decrease due to process j (equations (32) and (33)). This derivation concludes in the expression of equation (31), consistent with the one used by Rest in [47].

The concentration of interstitial loops increases due to growth of the di-interstitials population (and of clusters) and decreases when the interstitial loops become part of the network or when two loops coalesce (Equation (30)). The average diameter of interstitial loops can increase or decrease through climb, it decreases when smaller than average size loops are formed from di-interstitials (Equation (31)) or when loops unfault and it increases when loops coalesce.

As stated above, no differential equation is needed for the diameter of the cellular dislocation network as the diameter is determined using energy considerations via the following expression:

$$d_N = C_A C_\rho \sqrt{\frac{\pi}{f_\nu \rho_N}} \tag{40}$$

where f_ν is a function of Poisson's Ratio. The value of $C_A C_\rho$ is sometimes fixed to a value of 3, but in the present work that assumption is relaxed, introducing a variable parameter into the model. This expression and the value of $C_A C_\rho$ are further discussed in Appendix II.

Two more parameters should be further discussed; the dislocation climb and the production of clusters by radiation damage.

- **Climb**

There is not a unique definition for dislocation climb and its value depends strongly on how it is defined. Two things are generally accepted for this parameter: it increases with temperature and there must be a local supersaturation of one type of point defect (vacancy or interstitial) or a bias in the movement of one of those defects to the dislocation with respect to the other defect [41]. Taking this into account, the formula used to calculate the climb velocity was taken from the expression used commonly when modeling fuel swelling, but introducing a couple of modifications. That is,

$$\nu_I = \frac{2}{b_v}(z_i D_i C_i - z_v D_v C_v). \quad (41)$$

Eq. (41) shows the equation for the dislocation climb, which considers the difference of flux of both point defect types to the dislocation due to the effect of concentration, diffusivity and bias. If the net flux of vacancies and interstitials migrating to the dislocation is zero, then the dislocation will not have the possibility to climb.

It is essential to understand that the sign of the climb velocity is sometimes important:

- When calculating the mobility of a gliding dislocation, the absolute value is used.
- When calculating the growth or shrinkage of the loops, the sign is kept.

It is more difficult to define the bias for di-interstitial and small clusters. However the following expression is used:

$$\nu_{2i} = \frac{D_i C_i - 0.5 D_v C_v}{2a_0} \approx \frac{D_i C_i}{4a_0} \quad (42)$$

- **Cluster production rate**

The other parameter that must be detailed is the generation of di-interstitials by radiation damage. The model states that this parameter should exist, as clusters of vacancies and interstitials separate in space are formed during collision damage. These clusters have a high concentration of the defect type that constitutes it, thus there is a high probability that two defects stick together. However, there is a probability P_m for clusters to successfully grow into loops. This probability can be of the order of 10^{-3} [13].

Putting all these considerations together, one obtains

$$Q_{2i} = 2\dot{f}Q_{2i}^{0}P_m. \tag{43}$$

Equations for grain subdivision

Once the density of cellular dislocation network and its diameter have been evaluated, it is possible to calculate the stored energy introduced by them in the material. When the energy stored in the volume of the future recrystallized grain is equal to the surface energy needed to form the boundary of that new grain, a critical recrystallization diameter is obtained (Using equations (44), (45) and (46)).

$$d_{crx} = \frac{3\gamma_{GB}}{\Delta E_S} \tag{44}$$

$$\Delta E_S = \frac{\rho_N G b_v^2 f_v}{4\pi} \ln\left(\frac{C_A C_\rho}{d_N \rho_N b_v}\right) + \frac{G}{2}\left(\frac{b_v f_v d_N \rho_N}{2\pi C_A C_\rho}\right)^2 \tag{45}$$

$$\mathrm{G} = \mathrm{G}^0(1 - 1.09154 * 10^{-4}T)[0.9 - \frac{2}{\pi}\frac{0.1}{0.905}\mathrm{atan}\left(\frac{\dot{f}t - 5 * 10^{-26}}{2.5 \times 10^{-26}}\frac{20}{3}\right)] \tag{46}$$

Equation (44) is the expression for the critical recrystallization diameter, equation (45) is the expression for the stored energy in the dislocation network and equation (46) is an expression found for the shear modulus depending on the temperature and the fission density [28]. The third multiplicand of equation (46) is an approximation taken from Baron (Figure 2) [29].

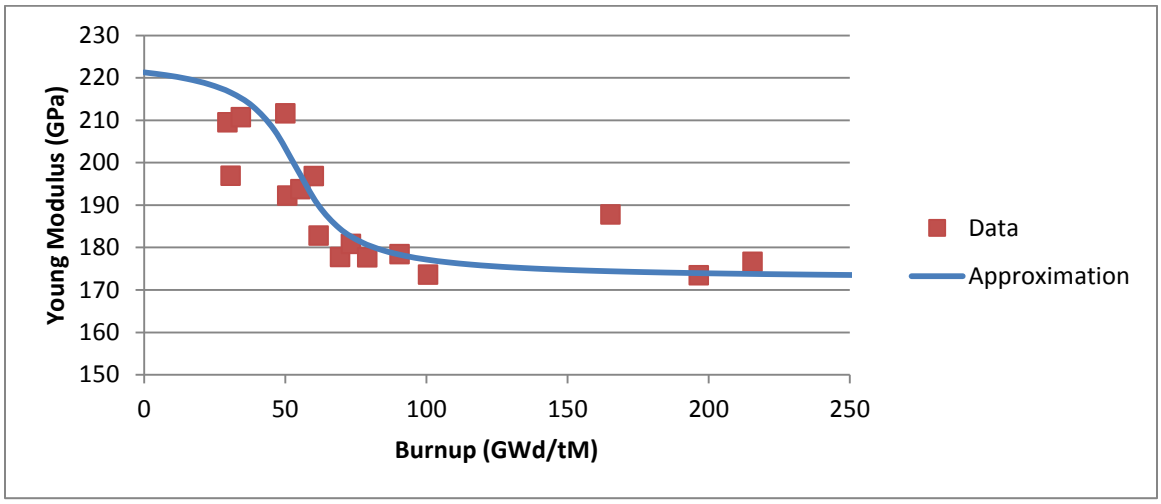

Figure 2. Dependence of Young Modulus on burnup (data and approximation after [29]).

Once the critical recrystallization diameter is calculated, it is necessary to know how many subgrains will be forming each new grain. It is proposed in this work that there would be a dependence of the Arrhenius type with respect to temperature for this number, apart from a relation with the stresses applied to the dislocations. A good guess for this relation is a formula similar to the one for steady state creep or five-power-law (Equation (47)). This hypothesis is based on the fact that creep is a mechanism by which dislocations move, especially at high temperatures. Therefore, the ability of the dislocations in the subgrain boundaries to move, forming a larger grain, might be explained with a similar expression (Equation (48)).

$$\dot{\epsilon} = C\sigma^5 e^{-Q/kT} \tag{47}$$

$$\mathrm{N_{subgr}} = \mathrm{C'}\sigma^5 e^{-Q/kT} \tag{48}$$

However, as the creep activation energy used in the five-power-law is generally equal to the activation energy for the diffusion of the self-interstitial atoms, some modifications were introduced to account for radiation enhanced diffusion. Hence, equation (48) becomes equation (49).

$$\mathrm{N_{subgr}} = \mathrm{C'}\sigma^5(C_v D_v + C_i D_i) \tag{49}$$

Moreover, there are some authors that recognize a formula like the one in equation (49), where an inverse relationship between the temperature and $\mathrm{C'}$is explicitly written [51].

$$\mathrm{N_{subgr}} = \frac{\mathrm{C'}\sigma^5(C_v D_v + C_i D_i)}{T} \tag{50}$$

Then, if the stress acting over the dislocation network is taken to be proportional to $\mathrm{b_v}\sqrt{\rho_N}$,

$$\mathrm{N_{subgr}} = \frac{\tilde{\mathrm{C}}(\mathrm{b_v}\sqrt{\rho_N})^5(C_v D_v + C_i D_i)}{T} \tag{51}$$

If the number of subgrains resulting from equation (50) is smaller than 1, then the subgrain diameter is used. If it is higher, then the recrystallized diameter would be the subgrain diameter multipied by the cubic root of the number of subgrains.

$$\mathrm{d_{crit}} = \begin{cases} \mathrm{d_N} & \mathrm{N_{subgr}} < 1 \\ \mathrm{d_N}\sqrt[3]{\mathrm{N_{subgr}}} & \mathrm{N_{subgr}} \geq 1 \end{cases} \tag{52}$$

As was already explained before, recrystallization is a very complex phenomenon that still has not been fully understood and there is no evidence that the amount of subgrains forming a grain will follow this expression; this is merely a semi-empirical formula used

to describe creep and, as such, it will be used as a semi-empirical expression for grain subdivision too.

Parameters

The unknown parameters present in the model are summarized in Table 1.

Table 1. Unknown model parameters.

In microstructural evolution model	
B	Relation between fission rate and generated free vacancy/interstitial pairs
Q_{2i}^{0}	Number of interstitial clusters produced by each fission
P_m	Probability of an interstitial cluster of growing into a dislocation loop
f_1	Dislocation annihilation rate constant
f_2	Rate constant for the joining of a dislocation to the network
p	Dislocation core radius multiplier
$\mathrm{C_A C_\rho}$	Constant in the dislocation network diameter
In the calculation of the grain subdivision initiation	
$\tilde{\mathrm{C}}$	Constant in the modified five-power-law
-	Correction of shear modulus due to burnup

This is a reduced list for UO_2, however when trying to apply the model to U_3Si_2, the number of parameters is increased and this list becomes more extensive.

Summary of new features in this model

In comparison with Rest's main model for grain subdivision, this work introduces several new features in an attempt to obtain better results describing recrystallization. These modifications are listed next.

Transient solution: this model considers that the time evolution of all the microstructural species is important to get a solution. No steady-state approximations are used. Apart from providing, hopefully, a more precise solution, it has the advantage of being able to be solved for varying conditions during irradiation.

Heterogeneous damage distribution: the effect of heavy ion damage in the distribution of the damage is included. This effect has two consequences that impact the nature of the damage produced. The first consequence is the generation of point defect clusters in the region where the collision occurs. The second consequence is a reduction of the efficiency of the damage forming mechanism.

Di-interstitial/cluster equation added: a new equation is added to the set of equations to describe the behavior of di-interstitials and clusters. These species are the precursors of the interstitial loops.

Dislocation bias equations used: an expression to calculate the sink strength of the dislocations and their bias was found in the literature and incorporated in the model.

Interstitial loop diameter equation: although Rest introduces this equation in one of his papers, more sources of change in the loop diameter were recognized and included.

Recrystallization criterion: The recrystallization criterion used by Rest was modified into one that allows the calculation of the critical values in a transient situation. A creep-like equation is proposed.

Effect of burnup in shear modulus: It was considered that the effect of radiation on mechanical properties used by the model can change with burnup. Therefore, an expression for the shear modulus that includes the effect of burnup is used. This effect, however, is only known for UO_2.

CHAPTER 6

Swelling calculation

Model Solution

From the equations described above, the set of differential equations describing the microstructural evolution was coded in Matlab and, using ode15s solver, it was solved in two steps: first it was solved for a fraction of a second step (10^{-6} s) during the first second of the evolution of the material under irradiation using the thermal equilibrium values as initial conditions. The results of this first step were used as initial conditions for the second solution using steps of 96 seconds.

The model for the microstructural evolution was solved for different fission rates and temperatures. The fission rates were obtained assuming quasi steady-state irradiation to calculate average fission densities from I^2S-LWR specifications. As it is proposed that self-shielding and resonance broadening causes a comparatively larger fission rate in the rim of the pellet, fission rates higher than the average were also considered. Regarding the temperature, typical PWR pellet temperature profiles were established. However, different combinations of temperature and fission rates will be studied looking for unexpected undesired conditions.

The I^2S-LWR plant parameter list, by the time this work was written, indicates 41.2 and 42 GWd/MTU average burnup and 58 and 64 GWd/MTU peak burnup for 12 and 18

month cycles, respectively. As the scope of this work is to study how much the pellet will swell under the worst condition, peak values are used. Pellets with the highest burnup are expected to be the ones with higher swelling.

The input of fission rate and density into the model is required in terms of fissions per m^3 per second and fissions per m^3; therefore burnup values were converted to the proper units, considering three years of irradiation in the reactor. To do this, one must know that each fission event provides approximately 3.2×10^{-11} joules and that a GWd is equivalent to 4.32×10^{15} joules. Then, the fission density per MTU is

$$\mathrm{FD_m} = BU \times \frac{4.32 \times 10^{15} J/GWd}{3.2 \times 10^{-11} J/fission} \tag{53}$$

where BU is the burnup and $\mathrm{FD_m}$ is the fission density per MTU. Then, to obtain the fission density per m^3, the fission density per MT of fuel is calculated and then multiplied by the density:

$$\mathrm{FD} = \mathrm{FD_m} \times \frac{n \times M_U}{M_{fuel}} \times 10^{-3} \frac{MT}{kg} \times \rho_{fuel} \tag{54}$$

where M_U is the molecular weight of the uranium, M_{fuel} is the molecular weight of the fuel, n is the amount of U in each molecule of fuel (1 for UO_2 and 3 for U_3Si_2) and ρ_{fuel} is the density of the fuel. The densities used were 96.5% of the theoretical densities ($i.e., \rho_{TD} = 10.97 \frac{g}{cm^3}$ for UO_2 and $\rho_{TD} = 12.2 \frac{g}{cm^3}$ for U_3Si_2)

It is important to remember that the fission rate and density will be considerably higher in the outer rim of the pellet due to self-shielding. Therefore, the average values will be

taken as the lower ones, while the fission rate and density at the rim will be assumed to be twice the average.

Hence, the values taken for the fission rates were 1.5×10^{19}, 1.75×10^{19}, 2×10^{19} and $2.5 \times 10^{19} \frac{fissions}{sec.m^3}$, which during three years of steady state irradiation will result in fission density values of 1.42×10^{27}, 1.66×10^{27}, $1.89 \times 10^{27}$and $2.37 \times 10^{27} \frac{fissions}{m^3}$, respectively. For the temperature, the values used to solve the model ranged from 600 K to 1400 K in 50 K increments. This range of temperatures was used to validate the model using UO_2 data, however the range is reduced when using the model for U_3Si_2.

Using equations (53) and (54), Table 2 and Table 3 were built relating the fission rate and the fission density (and burnup) by the end of irradiation for UO_2 and U_3Si_2 to use as guidance.

Table 2. Relation between burnup, fission density and average fission rate for 3 years in UO_2.

	0		2		4		6		8	
Burnup (GWd/MTU)	Fiss. density (fissions/m^3)	Fission rate (fissions/s.m^3)	Fiss. density (fissions/m^3)	Fission rate (fissions/s.m^3)	Fiss. density (fissions/m^3)	Fission rate (fissions/s.m^3)	Fiss. density (fissions/m^3)	Fission rate (fissions/s.m^3)	Fiss. density (fissions/m^3)	Fission rate (fissions/s.m^3)
10	2.51E+26	2.66E+18	3.02E+26	3.19E+18	3.52E+26	3.72E+18	4.02E+26	4.25E+18	4.53E+26	4.78E+18
20	5.03E+26	5.32E+18	5.53E+26	5.85E+18	6.04E+26	6.38E+18	6.54E+26	6.91E+18	7.04E+26	7.44E+18
30	7.54E+26	7.97E+18	8.05E+26	8.51E+18	8.55E+26	9.04E+18	9.05E+26	9.57E+18	9.56E+26	1.01E+19
40	1.01E+27	1.06E+19	1.06E+27	1.12E+19	1.11E+27	1.17E+19	1.16E+27	1.22E+19	1.21E+27	1.28E+19
50	1.26E+27	1.33E+19	1.31E+27	1.38E+19	1.36E+27	1.44E+19	1.41E+27	1.49E+19	1.46E+27	1.54E+19
60	1.51E+27	1.59E+19	1.56E+27	1.65E+19	1.61E+27	1.70E+19	1.66E+27	1.75E+19	1.71E+27	1.81E+19
70	1.76E+27	1.86E+19	1.81E+27	1.91E+19	1.86E+27	1.97E+19	1.91E+27	2.02E+19	1.96E+27	2.07E+19
80	2.01E+27	2.13E+19	2.06E+27	2.18E+19	2.11E+27	2.23E+19	2.16E+27	2.29E+19	2.21E+27	2.34E+19
90	2.26E+27	2.39E+19	2.31E+27	2.45E+19	2.36E+27	2.50E+19	2.41E+27	2.55E+19	2.46E+27	2.61E+19
100	2.51E+27	2.66E+19	2.57E+27	2.71E+19	2.62E+27	2.76E+19	2.67E+27	2.82E+19	2.72E+27	2.87E+19
110	2.77E+27	2.92E+19	2.82E+27	2.98E+19	2.87E+27	3.03E+19	2.92E+27	3.08E+19	2.97E+27	3.14E+19
120	3.02E+27	3.19E+19	3.07E+27	3.24E+19	3.12E+27	3.30E+19	3.17E+27	3.35E+19	3.22E+27	3.40E+19
130	3.27E+27	3.46E+19	3.32E+27	3.51E+19	3.37E+27	3.56E+19	3.42E+27	3.62E+19	3.47E+27	3.67E+19
140	3.52E+27	3.72E+19	3.57E+27	3.77E+19	3.62E+27	3.83E+19	3.67E+27	3.88E+19	3.72E+27	3.93E+19
150	3.77E+27	3.99E+19	3.82E+27	4.04E+19	3.87E+27	4.09E+19	3.92E+27	4.15E+19	3.97E+27	4.20E+19

Table 3. Relation between burnup, fission density and average fission rate for 3 years in U_3Si_2.

	0		2		4		6		8	
Burnup (GWd/MTU)	Fiss. density (fissions/m^3)	Fission rate (fissions/s.m^3)	Fiss. density (fissions/m^3)	Fission rate (fissions/s.m^3)	Fiss. density (fissions/m^3)	Fission rate (fissions/s.m^3)	Fiss. density (fissions/m^3)	Fission rate (fissions/s.m^3)	Fiss. density (fissions/m^3)	Fission rate (fissions/s.m^3)
10	2.94E+26	3.11E+18	3.53E+26	3.73E+18	4.12E+26	4.35E+18	4.70E+26	4.97E+18	5.29E+26	5.59E+18
20	5.88E+26	6.22E+18	6.47E+26	6.84E+18	7.06E+26	7.46E+18	7.64E+26	8.08E+18	8.23E+26	8.70E+18
30	8.82E+26	9.32E+18	9.41E+26	9.94E+18	1.00E+27	1.06E+19	1.06E+27	1.12E+19	1.12E+27	1.18E+19
40	1.18E+27	1.24E+19	1.23E+27	1.31E+19	1.29E+27	1.37E+19	1.35E+27	1.43E+19	1.41E+27	1.49E+19
50	1.47E+27	1.55E+19	1.53E+27	1.62E+19	1.59E+27	1.68E+19	1.65E+27	1.74E+19	1.71E+27	1.80E+19
60	1.76E+27	1.86E+19	1.82E+27	1.93E+19	1.88E+27	1.99E+19	1.94E+27	2.05E+19	2.00E+27	2.11E+19
70	2.06E+27	2.18E+19	2.12E+27	2.24E+19	2.18E+27	2.30E+19	2.23E+27	2.36E+19	2.29E+27	2.42E+19
80	2.35E+27	2.49E+19	2.41E+27	2.55E+19	2.47E+27	2.61E+19	2.53E+27	2.67E+19	2.59E+27	2.73E+19
90	2.65E+27	2.80E+19	2.70E+27	2.86E+19	2.76E+27	2.92E+19	2.82E+27	2.98E+19	2.88E+27	3.05E+19
100	2.94E+27	3.11E+19	3.00E+27	3.17E+19	3.06E+27	3.23E+19	3.12E+27	3.29E+19	3.18E+27	3.36E+19
110	3.23E+27	3.42E+19	3.29E+27	3.48E+19	3.35E+27	3.54E+19	3.41E+27	3.60E+19	3.47E+27	3.67E+19
120	3.53E+27	3.73E+19	3.59E+27	3.79E+19	3.65E+27	3.85E+19	3.70E+27	3.92E+19	3.76E+27	3.98E+19
130	3.82E+27	4.04E+19	3.88E+27	4.10E+19	3.94E+27	4.16E+19	4.00E+27	4.23E+19	4.06E+27	4.29E+19
140	4.12E+27	4.35E+19	4.17E+27	4.41E+19	4.23E+27	4.47E+19	4.29E+27	4.54E+19	4.35E+27	4.60E+19
150	4.41E+27	4.66E+19	4.47E+27	4.72E+19	4.53E+27	4.79E+19	4.59E+27	4.85E+19	4.65E+27	4.91E+19

Once the microstructural evolution during irradiation was obtained, this information was used to solve the second part of the model: the energy balance to determine if the grain would subdivide, and if it does, at which fission density. A code was written in FORTRAN that imports MATLAB solutions and calculates this fission density.

Solutions were validated for UO_2 using experimental data from the literature on the "rim effect". Once the validation was finished, the model was applied to U_3Si_2 and solved. If this solution is comparable to the solution for UO_2, then swelling would not be an issue that would forbid the use of this material, as the depth of restructured material from the pellet surface is only a few micrometers, while the grain size in the rest of the pellet remains the same or even larger ones could be formed by growth.

Parametric Analysis for Grain Subdivision Model

These equations have a number of parameters that are not completely defined. Therefore these parameters are varied to observe the effect on the results and assess the sensitivity of the results to each of these various parameters. These parameters are either unknown and should be determined in future work or they just add degrees of freedom to the model so that they can be fixed to values that allow a match to experimental data on high burnup structures in UO_2. Due to the complexity of the problem studied, these arbitrary parameters were deliberately accepted to account for deviations from ideal behavior and for the error introduced by the assumptions made. However, it is intended that these arbitrary parameters are kept to as few as possible.

Once a set of parameters is determined that describes correctly the high burnup structure, it was necessary to extrapolate these values to U_3Si_2 and, also, do the same for some parameters that were known for UO_2, but not for U_3Si_2.

FASTGRASS solution

The FASTGRASS manual defines it as a code for evaluating fission gas release in uranium-based fuels under normal and severe-accident conditions. Although this is the main objective of the code, it also provides an estimated value for the swelling due to gaseous fission products. FASTGRASS is a mechanistic code for predicting fission product behavior, which includes a prediction of the population of bubbles and the distinction between bubble types and their respective effects (bubbles in bulk material,

bubbles at grain faces and.at grain edges). Changes in the bubble distributions for each type of bubble are calculated through a balance of bubble coalescence and re-solution. By calculating the velocities of each type of bubble, a coalescence rate is calculated. Also, this allows the code to evaluate the transfer of bubbles to a different type [23, 24].

FASTGRASS assumes that bubbles that can migrate to grain boundaries would remain at the grain face, which constitutes a more stable location for bubbles to grow as they are less susceptible to re-solution. Conversely, a concentration of bubbles may be reached at which bubbles would be transferred from grain faces to grain edges. Bubbles at grain edges have a probability of undergoing long-range channeling and be released to macroscopic sinks (gap between fuel and cladding, central void, crack or macroscopic void). This sets a saturation value for the swelling buildup, as at some point the gases would be released.

Once all these effects are considered during the irradiation time, the swelling is calculated as the difference in volume between the initial and final volume, which is also equal to the sum of the volume of all the bubbles within the fuel.

Using FASTGRASS, with an appropriate input deck, it was possible to obtain values for swelling with a determinate time step until the critical fission density for grain subdivision initiation is reached. At that instant, the grain size is changed to the new recrystallized size and the code keeps performing swelling calculation at another time step until the cumulative modeling time reaches the end of irradiation.

Parametric Analysis for FASTGRASS

FASTGRASS is a code that strongly depends on the tuning of several parameters that describe different phenomena related to gas behavior, including diffusion coefficients, areal coverage necessary for bubbles to interconnect, probability of fission gas to be released and efficiency of re-solution. The version obtained through RSICC has default values for these parameters; however there is no proof that these were fitted values after validation. Therefore, it was necessary to find the adequate set of values that yield satisfactory results.

Apart from this, as the code is intended to be used to model UO_2, a further effort was needed to set the parameters to estimate values for U_3Si_2, which cannot be validated due to the lack of experimental data.

In Appendix V, there is a list of the different parameters under consideration. The sensitivity analysis was performed at temperatures, grain sizes and fission rates typical of PWR reactors for three years of irradiation.

Apart from the importance of each parameter, another conclusion which can be extracted from this analysis is that the sensitivity of the calculation with most of the parameters grows with increasing temperature and decreasing grain size.

It is worth to recall at this point that the sensibility analysis of FASTGRASS parameters is done to obtain approximate values of swelling that can be further used and refined with a better modeling of the swelling mechanisms. The primary objective of the thesis was to prove that there will not be a scenario of breakaway swelling which would forbid the use

of U_3Si_2 as fuel material in the I^2S-LWR reactor. For this reason, a fine tuning of these parameters was omitted because of lack of time.

1-D pellet model

Up to now, the mechanisms have been described by which a differential section of the pellet will swell. Also thus far presented was a description of the approach to be followed in calculating the magnitude of the swelling. However, the previous development considers a constant and homogeneous temperature and fission rate. Obviously, this is not the real situation of the pellet during irradiation in a power reactor. First of all, the pellet will go through transients (which may be slight or sharp and strong) in both fission rate and temperature. This effect will not be assessed in this work. On the other hand, the real engineering interest resides in estimating the swelling of the whole pellet. To approach this problem in a very simplified manner, radial symmetry of the pellet conditions will be assumed, and the cross section of the pellet will be divided into concentric rings over which temperature and fission rate will be constant.

To determine an appropriate thickness for the rings, it is important to consider typical shapes for the gradient of the burnup (that can be used to calculate fission rate) and temperature in the radial direction. As has already been explained, there is an increase of the fission rate towards the surface of the pellet, where the burnup can be around twice the average burnup. The thickness of the rim is usually less than 0.5 mm. (equivalent to less than 10 % of the pellet radius).

The 1-D model of the burnup distribution on the pellet was defined by three zones: a first zone, next to the surface, with a steep linear decrease of the burnup, a second zone with a quadratic transition between the first zone and the rest of the pellet and the third zone with a constant burnup. The burnup along the radius is normalized to match the average burnup.

Then, the burnup gradient is defined by: the relation between the peak burnup at the surface and the average burnup, the respective thicknesses of the first and the second zones and the slope of the burnup gradient in the first zone. The transition zone is defined by the continuity of burnup with the adjacent zones and by matching the derivatives in the interfaces between zones.

Defining the temperature gradient can be more complex; the temperature profile is known to vary during irradiation and assuming constant values is not completely correct. However, for the sake of this work, a hypothetical gradient is proposed with steep linear increase through the rim and, following it, a linear increase through the rest of the pellet until it reaching the centerline temperature. The high increase in temperature through the rim is expected to be caused by a reduction of the thermal conductivity due to the accumulation of damage in that region, enhanced by the increased burnup. This temperature slope is not expected at the beginning of the cycle. However the initial gap, which will not be closed by the swelling of the pellet at that moment, may have a comparable effect.

An example, albeit hypothetical, of burnup and temperature profile along the pellet is illustrated in Figure 3. As it can be seen in that figure and has been explained above, a value similar to the average burnup will be defined for most of the radius, while an increase is observed towards the edge of the pellet. This means that grain subdivision should be avoided for values of burnup in the range of the pellet average. This average should be chosen to be the average of the pellet with highest burnup in the core.

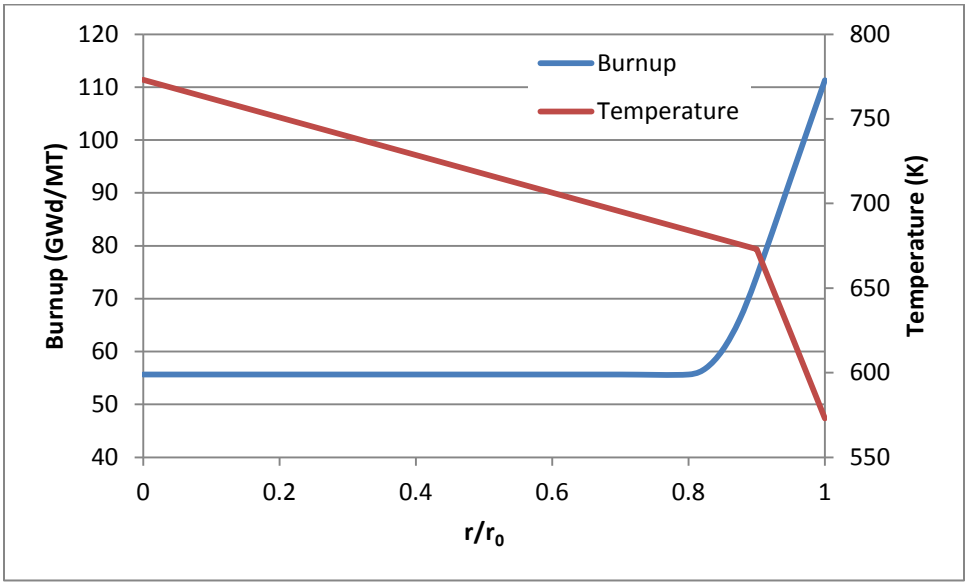

Figure 3. Hypothetical 1-D pellet burnup and temperature profile.

CHAPTER 7

Results and analysis

Parametric analysis results for UO_2

The model was solved for different temperatures and fission rates, varying the following parameters:

- Relation between fission rate and dpa/s (B)
- Dislocation core radius multiplier (p).
- Effective freely migrating defects produced per fission
- Clusters produced per fission
- Probability of a cluster to grow into a loop
- Constant in the equation for the number of subgrains forming a grain ($\tilde{C}$).

- **Constant of proportionality between the inverse of the square root of dislocation network density and subgrain diameter:**

The relationship previously stated in equation (40) is the object of intensive study for a great number of materials and UO_2 is not an exception. Studies using molecular dynamics have been carried out [41] and it was found that the diameter of the subgrains is, as the theory shows, proportional to the inverse of the square root of the dislocation density. It

is found that the constant of proportionality was equal to **3.5**. When plugging this value in the equation for UO_2, the compound parameter $C_A C_\rho$ if found to take the value **2.185**.

In this work, this value was taken as an unchanging standard when varying the rest of the parameters; however some simulations were run using different values.

- **Dislocation core radius multiplier**

The deformation energy of a dislocation line is infinitely large when calculated using the classical theory of elasticity, mainly because the stresses in the immediate neighborhood of the dislocation tend to infinity, but stresses are limited in a real crystal. Therefore, a cut-off radius is set that delimits the core region of the dislocation. Inside the radius the energy is calculated using atomistic considerations. The radius of this core is in the order of b_v [52].

As the appropriate dislocation core radius is unknown since it does not have an exact definition, in practice its definition turns out to be relatively arbitrary. In fact, it is more of a mathematical tool than a physical property, the practical use of which is motivated by the need to avoid the unexpected behavior of some values that are functions of it. In the same spirit, a proportionality factor p is defined to relate the dislocation core radius with the Burgers vector b_v.

The value of p, taking into account the above considerations and explanations, is found to be of the order of magnitude of 1.

- **Effective freely migrating defects produced per fission**

The number of effective freely migrating defects produced per fission event stands for the amount of defects that after being created do not end up as part of clusters and were not recombined during cooling down of the thermal spike or a short time later. The percentage of defects that survive can be around 1%, or even less, of the amount calculated by SRIM simulations (Appendix I).

- **Clusters produced per fission and probability of a cluster to grow into a loop**

These two parameters are treated as one in order to simplify the analysis. Creation of clusters directly during the damage cascades formation is critical for this model. This quantity increases the rate of nucleation of interstitial loops compared to nucleation solely from di-interstitials. However, as not all of the clusters successfully nucleate into loops, a probability of this happening is used to reduce the effective concentration of clusters.

- **Constant in the equation for the number of subgrains forming a grain**

This is the main fitting parameter of the model, used in the second part while calculating the number of subgrains that form a recrystallized grain. Mathematically, recrystallization occurs in the time step at which two curves representing diameters (equation (44) and (52)) cross. This constant moves one of the curves up or down until different intersections are registered for several temperatures.

This parameter can be analyzed with more detail by finding how it might be formed. First of all, it includes a constant (C') completely related with the creep behavior of the

material. This constant is multiplied by the power of 5 of any constant that is part of the stress component not explicitly contained in the equation.

If an approximate average stress of the dislocation network can be expressed as

$$\sigma_N \approx \sqrt{\frac{2Gf_\nu b_\nu^2 \rho_N}{4\pi E}} \tag{55}$$

then

$$\sigma_N \approx \sqrt{\frac{2Gf_\nu}{4\pi E}} (b_\nu^2 \rho_N)^{\frac{1}{2}} \tag{56}$$

Hence, referring to Equation (51)

$$\tilde{\mathrm{C}} \approx \mathrm{C}' \left(\frac{2Gf_\nu}{4\pi E}\right)^{5/2} \tag{57}$$

where E is Young's Modulus. Then, if two different materials were to be compared,

$$\frac{\tilde{\mathrm{C}}_1}{\tilde{\mathrm{C}}_2} \approx \frac{\mathrm{C}'_1}{\mathrm{C}'_2} \left(\frac{G_1 E_2 f_{\nu 1}}{G_2 E_1 f_{\nu 2}}\right)^{5/2} \tag{58}$$

Using the equivalency

$$\mathrm{E} = 2G(1+\nu) \tag{59}$$

Equation (58) becomes

$$\frac{\tilde{\mathrm{C}}_1}{\tilde{\mathrm{C}}_2} \approx \frac{\mathrm{C}'_1}{\mathrm{C}'_2} \left[\frac{(1+\nu_2) f_{\nu 1}}{(1+\nu_1) f_{\nu 2}}\right]^{5/2} \tag{60}$$

For the particular case of UO_2 and U_3Si_2

$$\frac{\tilde{C}_{UO_2}}{\tilde{C}_{U_3Si_2}} \approx 0.98 \frac{C'_{UO_2}}{C'_{U_3Si_2}} \quad (61)$$

Then, if the assumptions of this derivation are correct, the relation between $\tilde{C}$ for two different materials will be given by their steady-state creep behavior.

Validation with rim effect

Due to the large number of variable parameters and the scarcity of experimental data and their associated uncertainties, it was impossible to use traditional fitting tools, making it hard to find precise values for those parameters to fit the experimental data. Consequently, the mechanism used to find the appropriate set of parameters was to try to show trends similar to the expected behavior and, then, the parameters were finely tuned to fit the data.

The trend which the model tries to predict is finding grain subdivision at high burnup and intermediate temperatures (the temperature of the outer rim of the pellet), but not under other conditions.

Another constrain for the parameter fitting process is the recrystallized grain size, which must fit the sizes observed in the rim of high burnup pellets. These grains range from around 100 μm to 300 μm, and even to 800 μm, depending on the source of the data. It is complicated to relate each grain size with particular values of temperature and fission rate, especially considering that those values are not steady. But, again, the model tries to reproduce only the trends. It must also be said that in the experiments, between the grain

subdivision event and the experimental observation, there could be some grain growth, causing an overestimation of the grain size reported as recrystallizing diameter.

The set of fixed parameters that are used is given in Table 4.

Table 4. Parameters used for UO_2.

Measured			**Calculated**			**Estimated**		
Physical property	Value	Source	Physical property	Value	Source	Physical property	Value	Source
G (Pa)	8×10^{10}	[41]	r_{iv} (m)	8.2×10^{-9}	[47]	ϵ_v^m (eV)	2.4	[37]
ν	0.31	[41]	b_{vI}(m)	3.82×10^{-10}	[28]	ϵ_i^m (eV)	0.6	[37]
a_0 (m)	5.4×10^{-10}	[27]	b_{vD} (m)	3.82×10^{-10}	[28]	ν_v (s^{-1})	1×10^{13}	[53]
γ (J/m^2)	1	[28]	ΔV_v (m^3)	-2.2×10^{-30}	[41]	ν_i (s^{-1})	1×10^{14}	[53]
			ΔV_i (m^3)	6×10^{-30}	[41]			
			$C_A C_\rho$	2.185	[41]			

As previously stated, a three-year irradiation was simulated using different temperatures and fission rates. Then, the evolution of the microstructure was analyzed to find if recrystallization occurs with the recrystallization criteria detailed in Chapter 5. The parameter $\tilde{C}$, from equation (50), is varied until the two curves of diameter (the one obtained from the energy balance and the one obtained considering the amount of grains recrystallizing into one grain) intersect. This parameter is not changed between different temperatures and fission rate modeled cases.

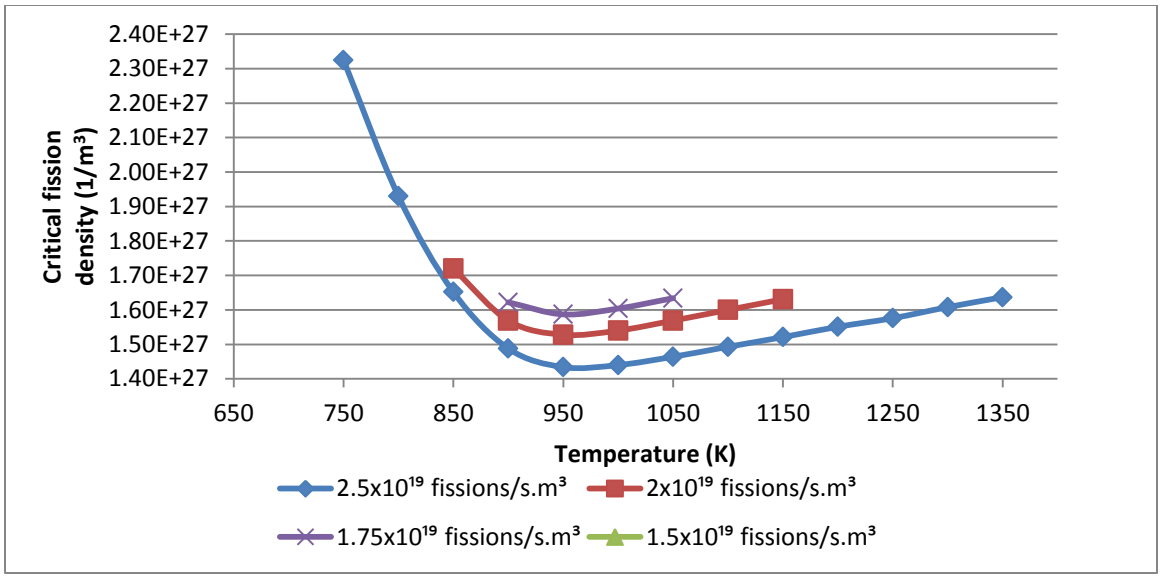

Figure 4. Critical fission densities for different fission rates and temperatures in UO_2.

In Figure 4 the effect of changing fission rate can be observed while the rest of the parameters are kept unchanged. While for 2.5×10^{19}, 2×10^{19} and $1.75 \times 10^{19} \frac{fissions}{sec.m^3}$ the fuel would recrystallize according to the curves shown, for $1.5 \times 10^{19} \frac{fissions}{sec.m^3}$ there is no curve because the fuel would no recrystallize at that fission rate. As anticipated, the fuel recrystallizes at lower temperatures and higher fission rates (and densities). When reaching the average fission rate, the fuel tends to stop recrystallizing.

This behavior seems to be consistent with the rim effect observed in UO_2 pellets, where recrystallization shows up in the periphery that is colder than the rest of the pellet. Higher temperatures would enhance annealing and the reordering of dislocations, keeping the dislocation density too low to result in recrystallization. However, as recrystallization is considered a thermally activated mechanism, there is a temperature at which the deformation (dislocation density) needed to achieve subdivision starts growing and

higher fission density is necessary. From Figure 4 it can also be concluded that the fission rate has an effect on reducing the fission density needed for grains to subdivide.

Recrystallization can be seen as a way by which the material heals itself. If the temperature is reduced to even lower temperatures compared to the ones found in power reactors, the accumulation of damage may be unconstrained, leading to a situation similar to that of an amorphous material.

It is important to note that, apart from the effect of the temperature, high burnups and fission rates are required, conditions only found in the periphery of the pellet. For fission rates and burnup in the range of the pellet average, recrystallization would not occur. Also observed is a progressive growth of the depth of the rim with burnup; it is possible that this could be explained by the depletion of the first micrometers from the pellet surface, pushing the self-shielding annulus to the interior of the pellet.

It must be understood that radiation enhanced recrystallization is a compound effect of increased dislocation density and increased point defect concentration. If a parallel is to be drawn between the rim effect and grain refinement in cold-worked metals, higher dislocation densities reduce (in both cases) the recrystallization temperature; but radiation also increases the speed at which diffusion mechanisms act, requiring even lower temperature.

Together with the critical fission density, the recrystallized grain diameter was found. The results were plotted in Figure 5. It can be seen that the diameter goes from 200 nm at

low temperatures to over 350 nm at higher temperatures. This is consistent with the available experimental data [54].

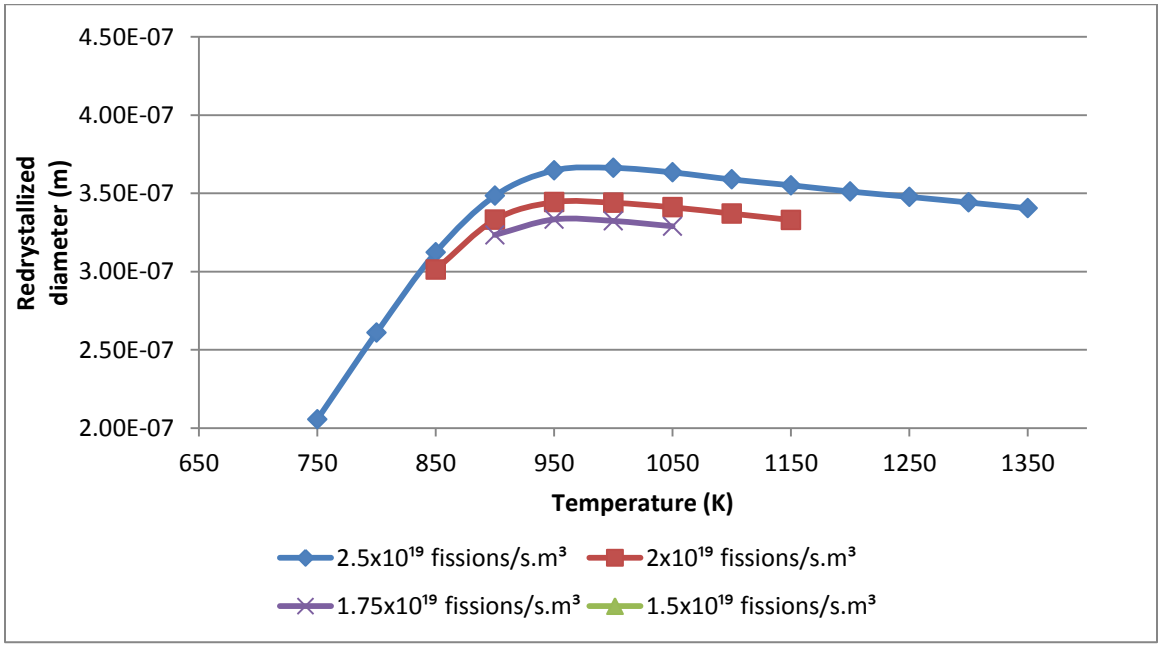

Figure 5. Recrystallized diameter for different fission rates and temperatures in UO_2.

These results are provided for several hypothetical cases. However to apply the model to the real pellet situation, the 1-D pellet model is used. With this, a specific temperature would be correlated with its specific fission rate and radial position in the pellet. This approximation will provide information on the extent of the rim, which should fade away a few hundredths of millimeters from the pellet surface.

Although the model performs well to predict the rim effect, the concentration of loops predicted is higher than expected. This is considered an important flaw of the model,

however state-of-the-art models for the behavior of the microstructure have the same flaw [55]. This means that the models overestimate the production rate of loops and underestimate the rate at which loops join the network. A satisfactory solution has not been found to make the model predict expected values for the loop concentration and be properly validated with rim effect data; but with some modifications, it was possible to predict with good results the microstructural evolution reported in the previously cited paper (See Appendix IV).

It is interesting to note that the effect of variations in the migration activation energies is negligible. This can be explained since the evolution of the extended defects is mainly characterized by the products $D_v C_v$ and $D_i C_i$, which are defined by radiation enhanced diffusion and tend to stabilize, at constant temperature, at the same value, whatever the diffusion coefficient.

Solution for U_3Si_2

Once established that the model results follow the trends of the observation of the rim effect in the UO_2 fuel pellets, solutions are obtained for different sets of parameters for U_3Si_2. Table 5 details some of the standard parameters used in the simulations.

Table 5. Parameters used for U_3Si_2.

Measured			Calculated			Estimated		
Physical property	Value	Source	Physical property	Value	Source	Physical property	Value	Source
G (Pa)	3.3×10^{10}	[56]	a_0 (m)	3.4×10^{-10}	[1]	ϵ_v^m (eV)	0.9	[1]
ν	0.17	[56]	Ω (m^3)	1.4×10^{-28}	[31]	ϵ_i^m (eV)	0.3	[d]
			b_{vI}(m)	3.82×10^{-10}	[a]	ν_v (s^{-1})	1×10^{13}	[53]
			b_{vD} (m)	3.82×10^{-10}	[a]	ν_i (s^{-1})	1×10^{14}	[53]
			ΔV_v (m^3)	-3.08×10^{-29}	[b]	r_{iv} (m)	8.2×10^{-9}	[c]
			ΔV_i (m^3)	2.52×10^{-28}	[b]	γ (J/m^2)	0.5	
			G (Pa)	3.3×10^{10}	[56]			

[a] Calculated for $\overrightarrow{b_v} = (1\ 1\ 0)$.
[b] Calculated after [57].
[c] Same value as UO_2 used.
[d] Rough estimation multiplying by the ratio between melting temperatures of U_3S_{i2} and UO_2

After solving the model with the parameters from the table, a similar solution from the one in the case of UO_2 is obtained, without modifying the constant from the amount of subgrains recrystallizing in a new grain. Although this parameter in totally unknown, it can be presumed, on one hand, that it may be higher than for UO_2 because of higher creep in metals compared to ceramics. On the other hand, stress produced by the same dislocation density will be lower due to a lower shear modulus. If we remember that stress is affected by a fifth power, this difference can be important.

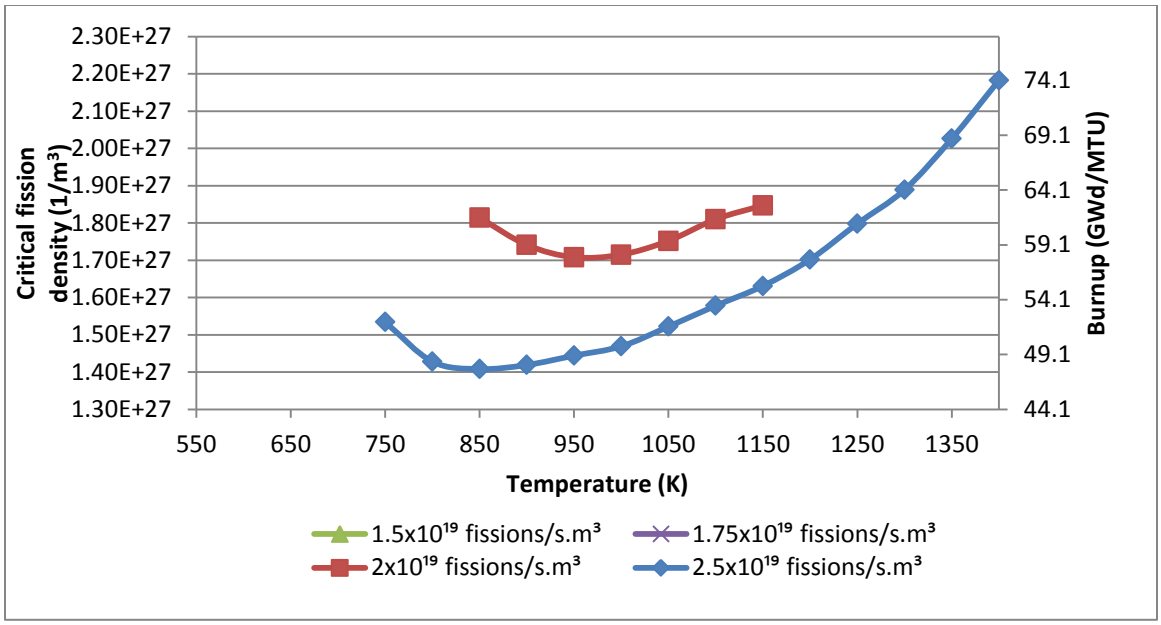

Figure 6. Critical fission densities for different fission rates and temperatures in U_3Si_2.

As it can be seen, only at very high fission rates (on the order of the rates at the rim), the fuel recrystallizes. Also, there is an upper and lower temperature limit which can be seen in the previous figure. The model solution is plot for temperatures from 550 K to 1400 K, thus the discontinuity of the lines show that subdivision only occurs within the range of temperatures at which the line is shown.

However, this solution considers that the dependence of the shear modulus with burnup is similar to the one in UO_2. If this correction is not assumed, the solution obtained is the following:

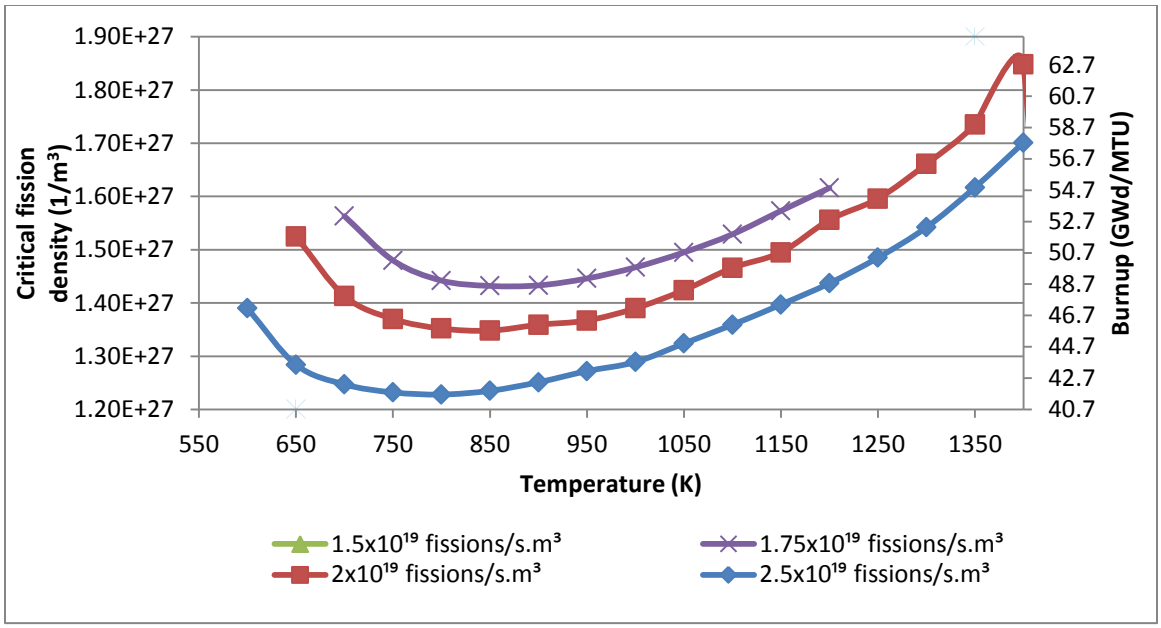

Figure 7. Impact of removing the effect of burnup on the shear modulus.

This correction makes, thus, an important difference in the critical rate. Fortunately, at low fission rates, comparable to the average value, the fuel will still not recrystallize.

Another parameter that has a notorious effect in the result is the constant defining the relation between the network dislocation density and the network cell diameter ($C_A C_\rho$). The effect of increasing this parameter results in higher critical fission densities. If we assume that for U_3Si_2 this parameter will be between the value for UO_2 and the value for metals, we can guess that it may be higher than the value used for UO_2. Figure 8 shows the critical fission density for $1.75 \times 10^{19} \frac{fissions}{sec.m^3}$ varying $C_A C_\rho$. This constant is doubled in the upper curve.

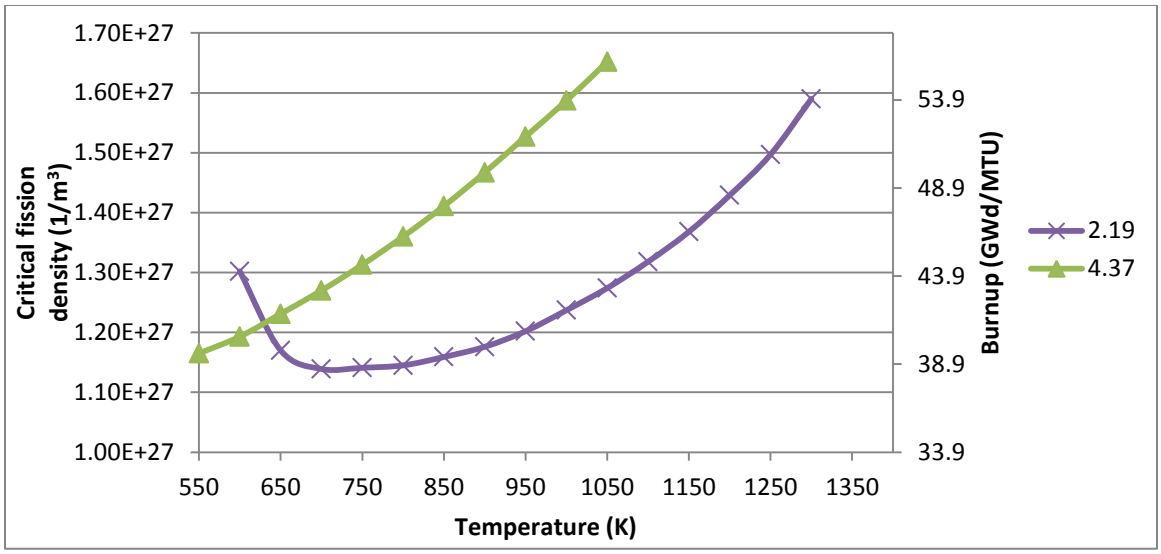

Figure 8. Effect of the parameter $C_A C_\rho$.

It is still necessary to model properly the damage produced by fission fragments in the material. Variations in the damage efficiency, the cluster production rate and the cluster nucleation probability have a considerable effect on the final result. An increase in the amount of freely migrating point defects production rate impacts the radiation enhanced diffusion, increasing dislocation mobility and promoting recrystallization. An increase in the rate of loop nucleation from clusters raises the population of dislocations and would accelerate recrystallization. Figure 9 shows the effect of increasing the amount of freely migrating defects produced per fission event. Larger rates of production enhance recrystallization.

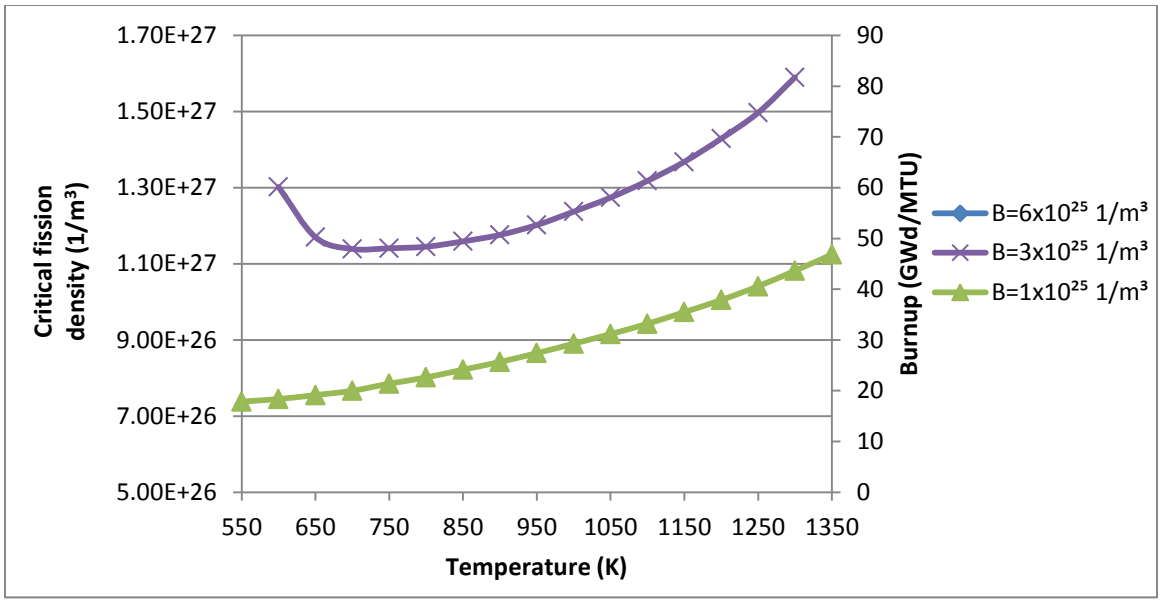

Figure 9. Effect on critical fission density of the amounts of freely migrating defects produced.

The value of the migration energies of the point defect does not have any visible effect in the results, which the same behavior as in the case of UO_2.

FASTGRASS calculations

A number of cases were run in FASTGRASS for several parameters to show the effect in the swelling of the recrystallization.

The main disadvantage of using FASTGRASS to do these calculations is that it will not be able to provide a good estimation of the bubble size, given that the bubbles observed in the rim do not belong to any class considered by the code (lattice, grain face, grain edge). Instead, these bubbles may correspond to part of the released gas. As most of the

porosity at the rim is composed by these types of bubbles, the release probability is reduced until similar values of porosity are obtained.

Nevertheless, at least in a qualitatively manner, it is possible to evaluate the effect of grain size in the migration of gas atoms to the surface of the grains and how the reduction of the diameter enhance swelling.

It must be highlighted that the final swelling calculation is independent of the fission density at which the grain recrystallized, as it can be seen in Figure 10. This is justified as most of the fission gases produced are still present in the grain lattice. Only when the grain subdivides, the gases find their way out of the lattice to the grain face. The kinetic of the gas migration out of the grain after subdivision is fast, so no transition between the two states is observed. From this, it can be extracted that the relevant information is if the grain subdivides or not during its irradiation, but not when.

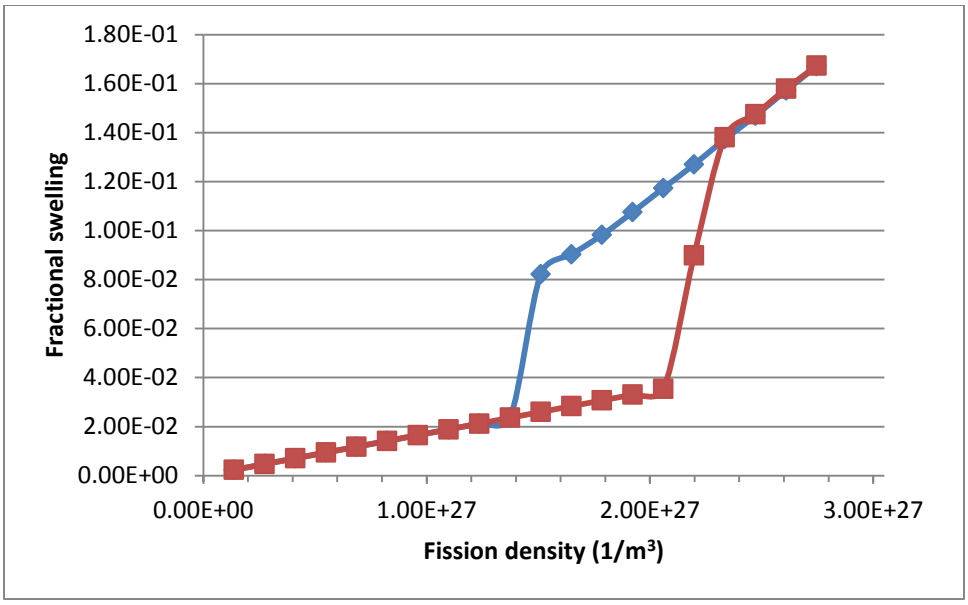

Figure 10. Swelling at identical condition with different recrystallizing fission density.

Figure 11 shows the effect of temperature in the swelling for recrystallized grains in UO_2 with a discharge burnup of 69 GWd/MTU. The grain subdivision is arbitrarily assumed to occur at the three fourth of the lifetime (51.75 GWd/MTU). Although this value may be too low, as it was shown before, the swelling seems to be independent of the fission density at which the grain may subdivide.

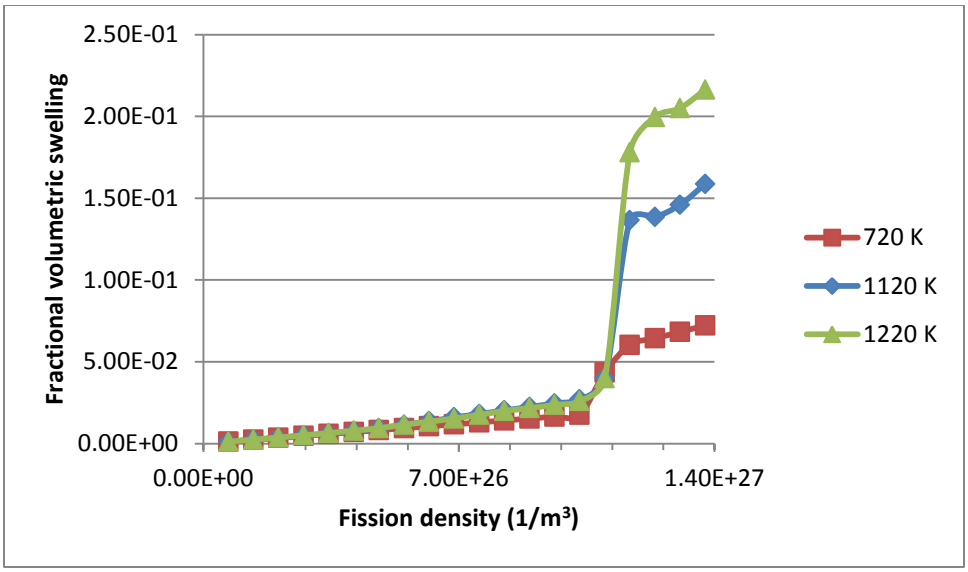

Figure 11. Swelling in UO_2 for different temperatures.

When comparing the swelling of UO_2 and U_3Si_2 after subdivision, a higher swelling is observed in the latter. This is caused by a lower surface tension, which leads to higher equilibrium bubble sizes for the same amount of gas at the same pressure and temperature. This may be one of the most important disadvantages of U_3Si_2 from the swelling point of view.

Figure 12 displays a similar case as Figure 11, but for U_3Si_2. It can be easily seen that the swelling is much higher if the whole fuel recrystallizes. Still these solutions do not consider fission gas release, as the evidence from the rim effect shows that the gas stays in the pellet located in large pores and contribute to swelling. If the complete release of the gases from the pellet is enhanced at high temperature, then these will be much smaller.

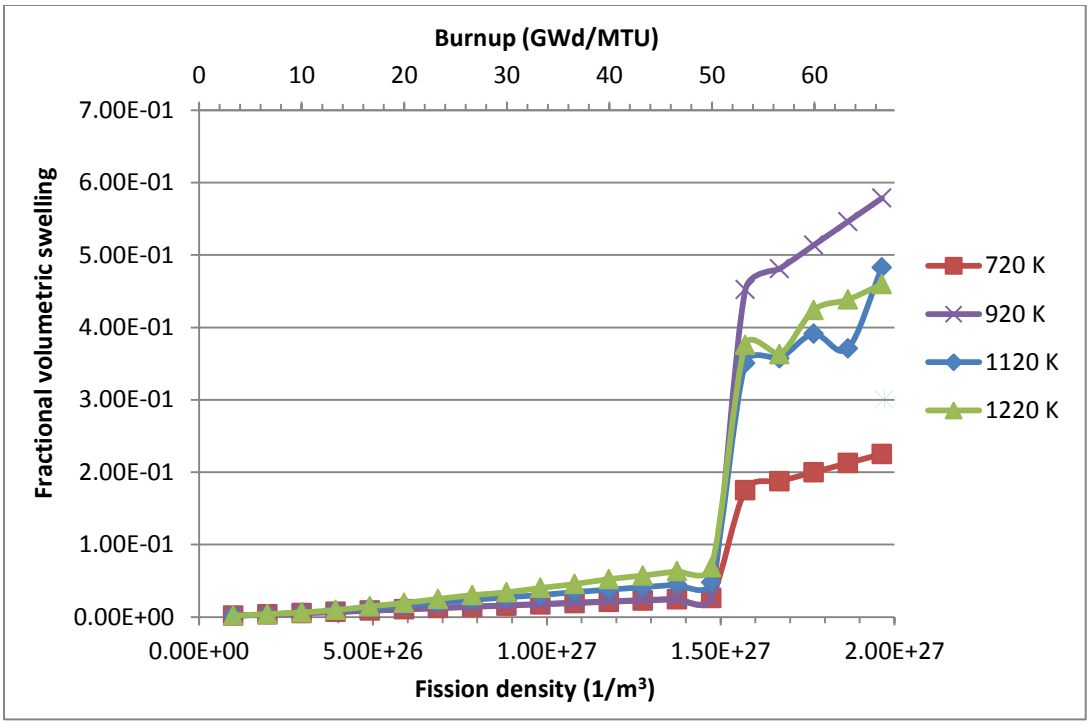

Figure 12. Swelling in U_3Si_2 for different temperatures.

Then, assuming that Figure 12 shows a qualitative behavior of the fuel swelling, if the recrystallizations extend through the entire pellet, the dimensional change will be high and unacceptable. Therefore, it can be determined that if the pellet recrystallizes at burnups below the average value, then the fuel cannot be used.

If the fuel does not recrystallize, then the swelling calculated with FASTGRASS will be much lower, as it can be seen in Figure 13.

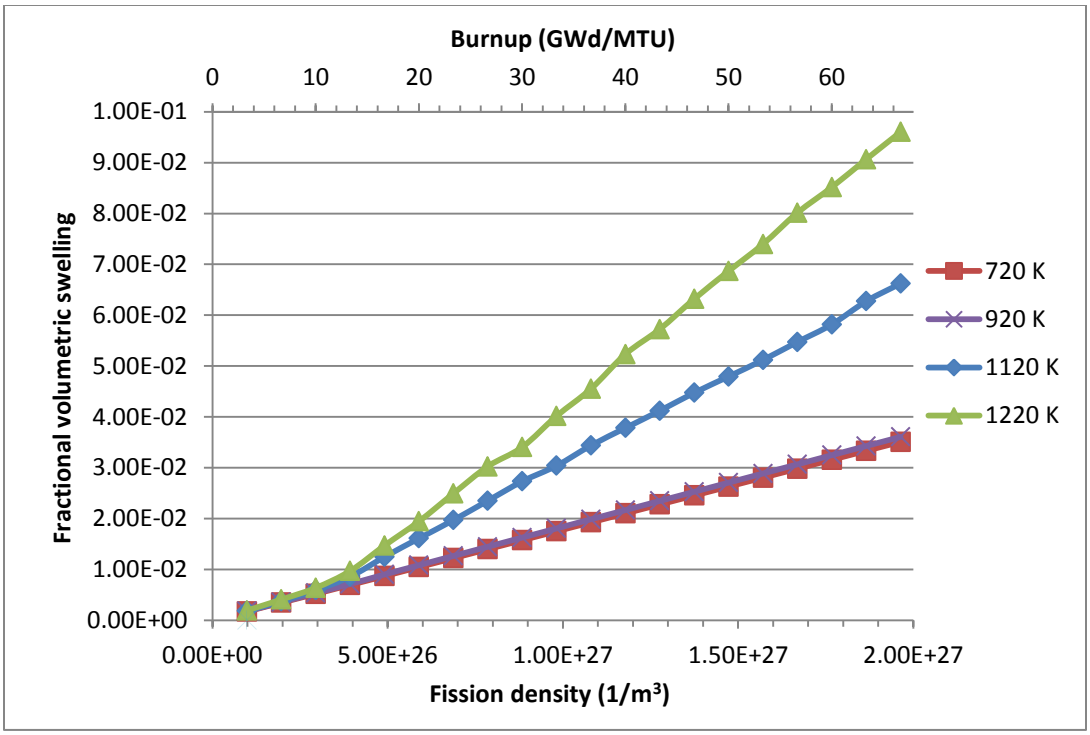

Figure 13. Swelling of U_3Si_2 without recrystallization.

The effect of the grain size can also be calculated using FASTGRASS. Figure 14, Figure 15 and Figure 16 show that the swelling of recrystallized fuel with submicronic size will be higher than the swelling for large grains. However, a size seems to exist for which the swelling reaches a maximum and then decreases. This effect will not have a practical application though, as it is probably difficult to control the recrystallized size in the reactor, but it is still worth mentioning. The effect of grain size on swelling will be milder as the fission gas release probability (through the parameter BVCRIT) is increased. The reason for this is that the gas released from the grain will easily abandon the pellet.

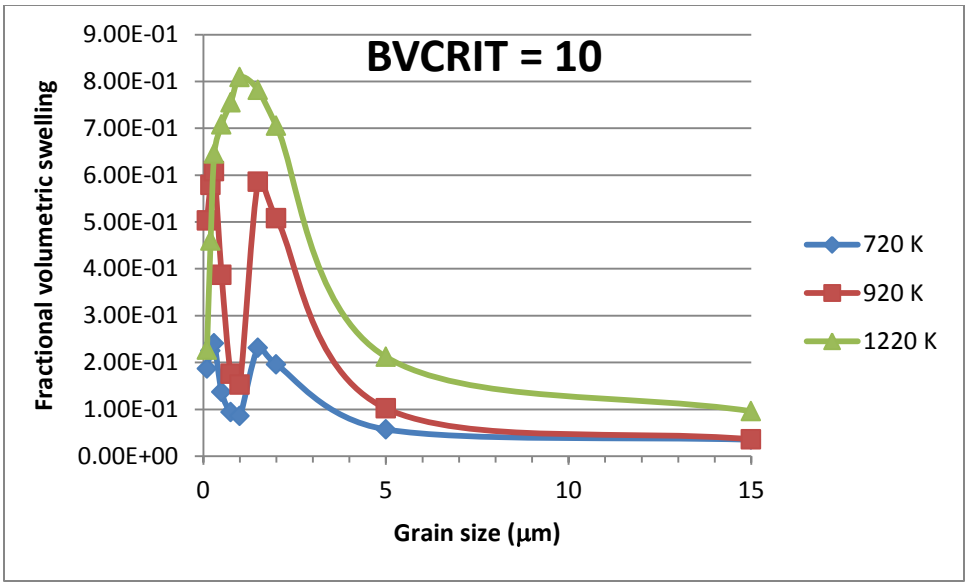

Figure 14. Dependence of the swelling with the recrystallized grain size without FGR.

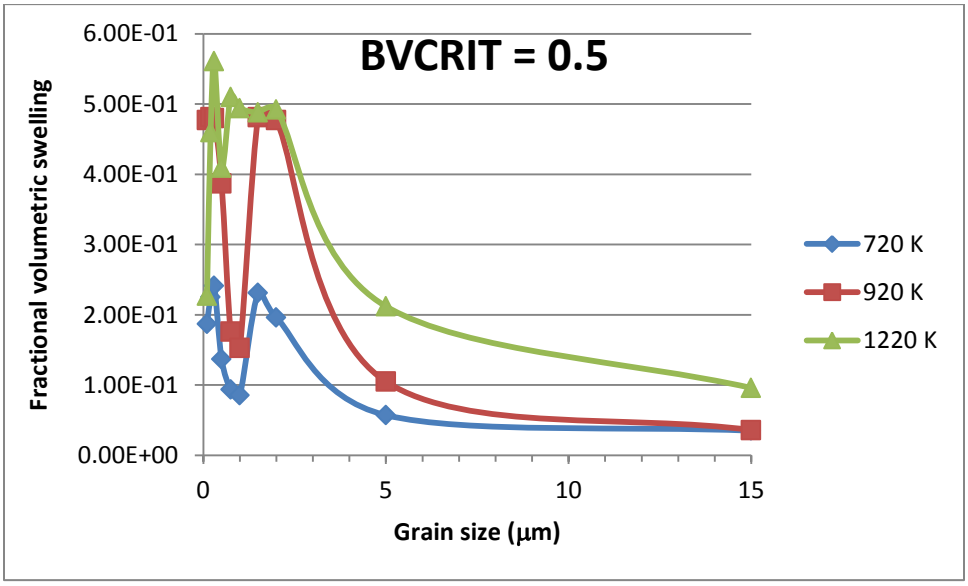

Figure 15. Dependence of the swelling with the recrystallized grain size with mid FGR.

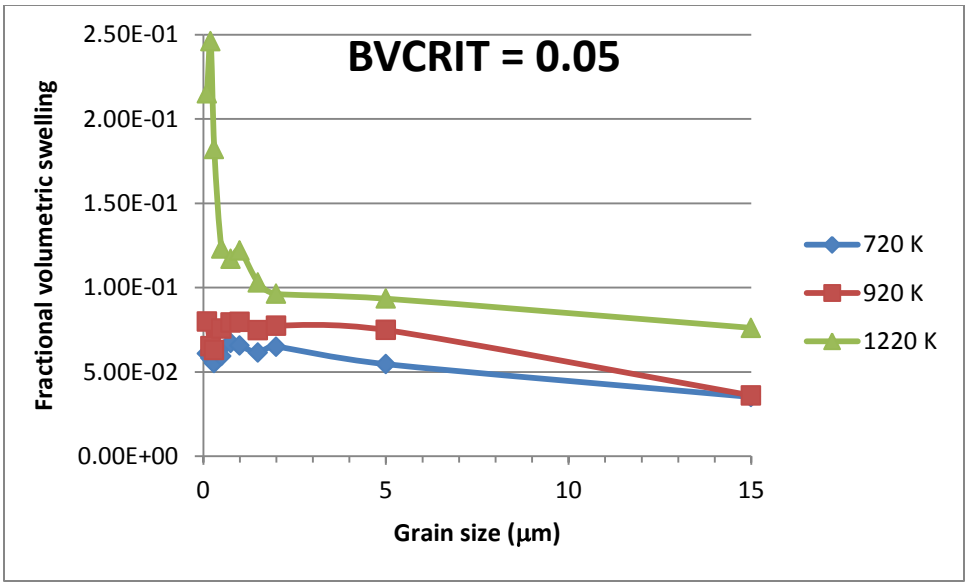

Figure 16. Dependence of the swelling with the recrystallized grain size with high FGR.

Thus, it is observed that fission gas release has the property of limiting the swelling. If the probability of fission gases to be released is increased, then the swelling will rapidly saturate for low values. Figure 17 shows the swelling for four temperatures setting the FASTGRASS parameter BVCRIT to 0.05.

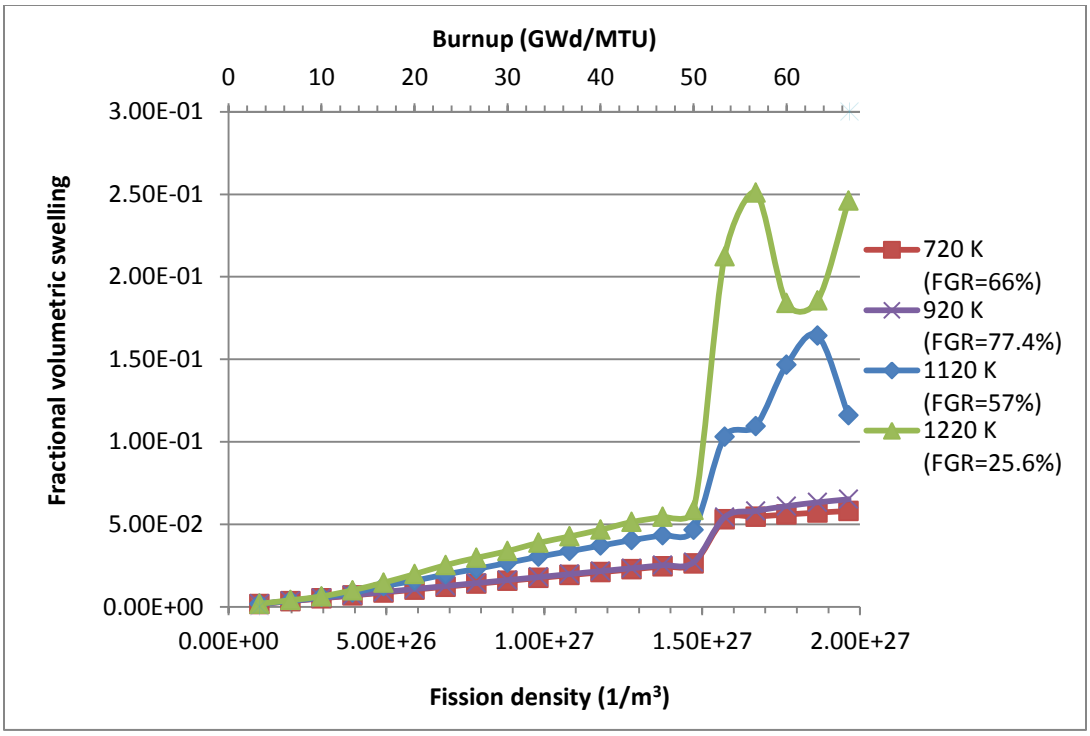

Figure 17. Swelling of recrystallized U_3Si_2 with high fission gas release.

The swelling values in the last figure are smaller than the ones shown in Figure 12. This shows the importance of predicting the fission gas release, especially at high temperature.

Swelling for a lower, but still not negligible, fission gas release was calculated too. The result can be seen in Figure 18.

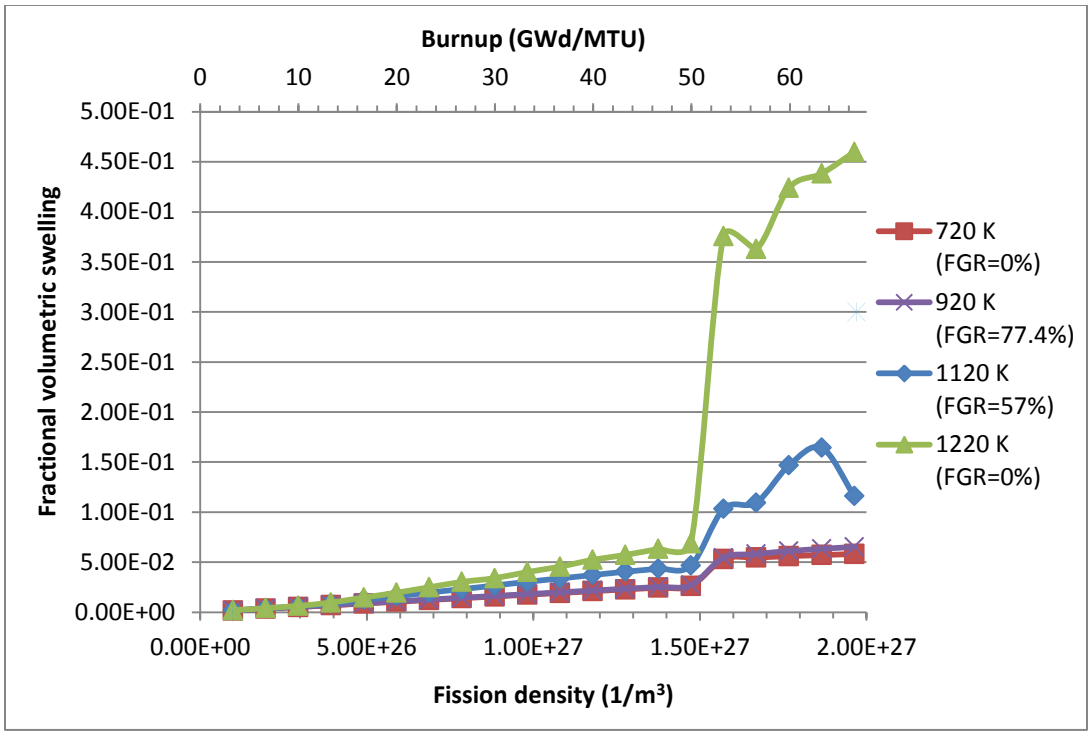

Figure 18. Swelling of recrystallized U_3Si_2 with mid fission gas release.

The mechanism used by FASTGRASS to calculate the fission gas motion from the lattice to the grain faces and from the grain faces to grain edges seems to impact the behavior of the swelling in an erratic way. The effect of temperature is not monotonous, indicating that more than one mechanism are competing with each other. While for high fission gas release, the swelling peaks at a temperature close to 920 K, if the release probability is decreased, that peak disappears. However, the percentage release at that temperature does not change. This behavior is not fully understood and should be further investigated.

Solid fission fragment calculation

According to what was explained in previous chapters, it is not the aim of this work to model the solid fission fragment swelling. However, some consideration will be given to its contribution to the swelling.

It is important to consider that, if the solid fission fragment swelling is due to the elastic strain caused by the extra atoms created during fission, that strain should be correlated to the mechanical properties of the material.

Therefore, if the fission products produce approximately the same stress on the crystal lattice due to its presence both in UO_2 and U_3Si_2, the strain it will generate will be proportional to the inverse of the shear modulus. As the shear modulus of U_3Si_2 is about half of the one of UO_2, the strain would be around the double of the values calculated for UO_2.

Without any further development and just to propose a probable mechanism to extrapolate the expression from UO_2, according to MATPRO [20], to U_3Si_2, solid fission fragment swelling for UO_2 and values proposed for U_3Si_2 were calculated and plotted, together with an expression provided by Kim [58].

The proposed solid fission fragment swelling is compared with values for the swelling observed by Shimizu [56] during high temperature irradiation of U_3Si_2.

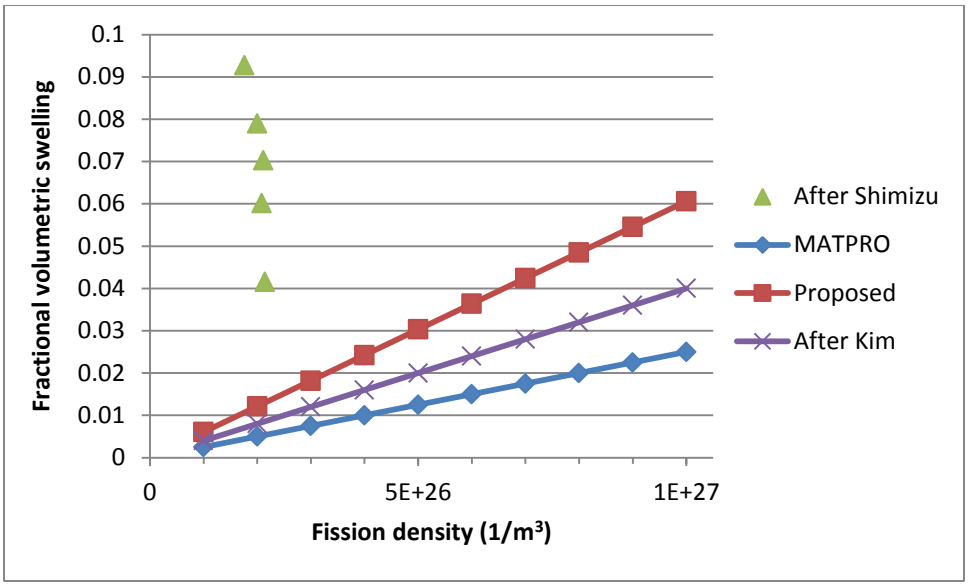

Figure 19. Solid fission fragment swelling from different sources compared experimental data [56].

However, despite being a plausible adaptation of the solid fission fragment swelling, looking at Figure 19, it can be concluded that this effect cannot completely explain the swelling observed by Shimizu [56]. Still summing up the gaseous swelling to the proposed solid swelling, the values obtained by Shimizu cannot be reached (Figure 20).

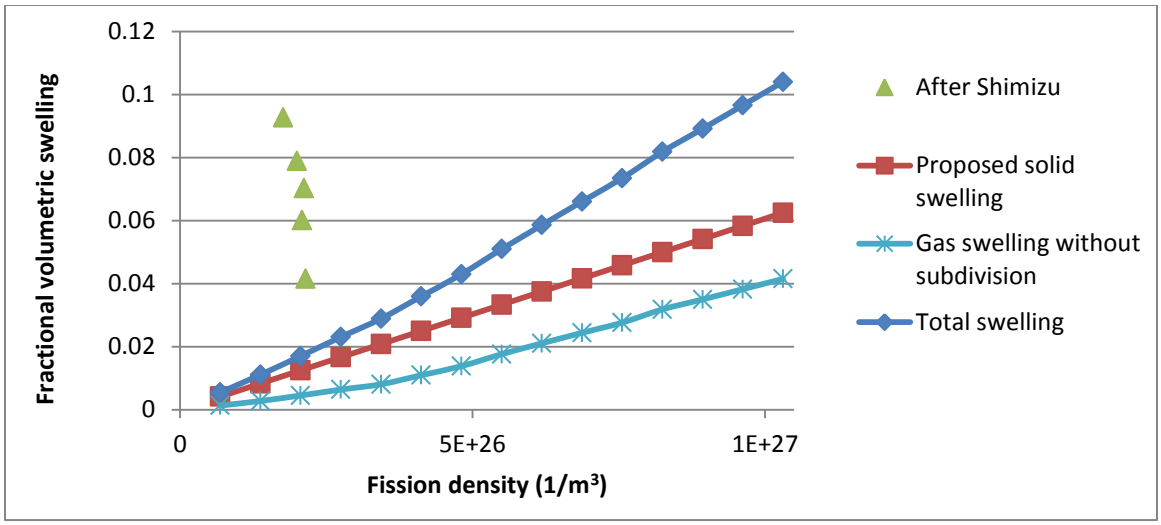

Figure 20. Total swelling compared to experimental data [56].

After this analysis, it can be concluded that there are to possibilities; either U_3Si_2 subdivides very soon during irradiation or the measurements from the literature were not too precise. From the images provided by Shimizu, some grain subdivision can be observed, although the author attributes that structure to a third phase on an interaction layer. It is possible that this presumed third phase is in fact recrystallized U_3Si_2 towards the surface of the pellet due to the increased fission density from self-shielding. Though the thickness of this layer might be small, the high temperature of the irradiation may have enhanced the swelling.

CHAPTER 8

Relation between swelling and other properties

- **Fission gas release**

Fission gas release is enhanced by grain subdivision as gas atoms reach a grain boundary more easily (because of increased proximity). Despite this, further modeling should be carried out in order to determine the fate and destination of the released gas. From the observations on the rim effect, it can be concluded that part of the released gas is collected within macroscopic pores of about 1 μm average effective diameter. These pores are about 10 times larger than the subdivided grains, a fact that indicates that they are not bubbles formed at the edges of the subdivided grains. This observation conflicts with the belief that the latter (grain edges) are the last containment of the gases before being released from the pellet. Experimental observations also concluded that part of the gas is effectively released from the pellet (most probably to the gap). Regardless of this, the porosity in the rim is much higher than the expected saturation gaseous swelling detailed in MATPRO.

The mechanism by which the intergranular gas is pre-released to large pores should be further investigated. A possible mechanism is proposed here that should be studied for confirmation (or denial): it is proposed that grain subdivision increases the tortuosity of the path the gases must go through, increasing the pressure drop of the gas moving along

that path. The mechanism might be similar to the one of gases passing through porous media in which Darcy's Law or Knudsen model are suggested.

- **Thermal Conductivity**

Dimension (e.g., swelling) is only one of the properties that can undergo changes during the microstructural evolution of the fuel under irradiation. The growth of a second phase (bubbles) in the fuel can strongly affect in a negative way (i.e., decrease) the thermal conductivity. However, there is evidence that recrystallization, by reducing the concentration of defects, increases the thermal conductivity.

The presence of gas in the large pores formed after grain subdivision should be assessed on whether it has a negative effect compared to an originally larger gap. If the reduction of the thermal conductivity due to the increased porosity is counterbalanced by a better contact between the pellet and the cladding, then the porosity might not be the most important issue.

- **Pellet-to-clad interaction**

If the effect of porosity in thermal conductivity is counterbalanced by a better contact between pellet and cladding, then the main issue would be the stresses from the pellets acting on the cladding. If the unrestrained swelling is too high, then the pressure applied by the pellet onto the cladding may be higher than the yield strength of the cladding which would fail.

CHAPTER 9

Inclusion of correlation in fuel performance codes

In FRAPCON, the swelling routine is named FSWELL. This routine includes swelling due to both solid and gaseous fission fragments. The swelling rates used are taken from MATPRO. The swelling correlations contained in MATPRO are empirical and were calculated after different authors. Swelling due to gaseous fission fragments tends to be small; this is explained by the small saturation swelling reached due to a high probability of fission gas release once the bubbles are formed at the grain boundary. However, FRAPCON does not include in its swelling expression the effect of grain size and the experimental data it is based on was probably obtained from large grains cases. The grain size reduction, however, has a substantial effect on the swelling saturation, as it can be noticed from the high burnup structures, where porosity can be around 15%.

The model presented here is not useful for performance codes such as FRAPCON, which has a simple correlation coded in its algorithm. However, it may be expected that if no subdivision occurs throughout the whole pellet, swelling values would be similar to the ones for UO_2 and a proper correlation from experimental data would thus be obtained. If the whole fuel pellet subdivides, ignoring the fact that the fuel will probably not be suitable for power reactors, the calculation of the swelling must be reconsidered, including a decrease in the fission gas release, if any, that would lead to an increase in the saturation swelling.

On the other hand, a code such as BISON could be made to include the differential equations for determining the instant at which grains subdivide, and solve the equations, coupled, with an account for all the variables that could affecting the result (i.e., influence swelling). This would provide a more accurate, but rather complex solution. To simplify the task and minimize the effort, a correlation like the one used in FRAPCON can be included instead [33].

CHAPTER 10

Conclusions

Modeling of microstructural evolution under irradiation is one of the major challenges in the construction of fuel performance models. This is even more so for novel fuel forms where only limited experimental data are available. The combined effects of atomic and mesoscale phenomena in highly heterogeneous configurations mandate the introduction of several assumptions and simplifications that deteriorate the fidelity of the models and decrease the accuracy of predictions. Analyses at lower scales are implemented in order to estimate parameters that are used in larger scale model equations. Also, the lack of consistent and well-known parameters and the uncertainty about details of physical conditions increase the complexity of the validation process.

Based on these considerations, an effort has been made to model the formation of subgrains in nuclear fuels due to the grouping of dislocations and their evolution into cell walls and subsequent local material recrystallization.

A principal outcome of this thesis is the development of a novel model for recrystallization. Its predictions were compared to the observations from the subdivided rim of UO_2 high burnup fuels, and a satisfactory agreement was observed. The model was then used, in an extrapolated way to estimate the extent of subdivision in U_3Si_2.

The importance of accurately predicting the onset of grain subdivision stems from the importance of grain boundaries to act as sites for bubble growth and hence to favor material swelling, as was proven in prior work by others. Thus, the work presented in this thesis provides a rational foundation for modeling the swelling of fuels under irradiation since it does predict the onset of crystal grains subdivision or recrystallization. The distinguishing feature of the present work is that it relies on much fewer adjustable parameters and adheres to physical models considerations to as wide an extent as possible.

From the temperature dependence of the recrystallization phenomenon that is observed in the results of the model developed here, it is important to highlight the finding that the recrystallization front advances from the colder part of the pellet to the hotter. This is an advantage, as the effect of recrystallization on swelling is lower at lower temperatures, at which the literature shows that a different mechanism appears to dominate. Consequently, the thickness of the rim must be large to reach temperatures at which it could considerably affect swelling.

Although the model was validated for UO_2, some parameters were arbitrarily chosen, as no constraint could be identified that imposes a value or even a specific range of values. For this reason, it is recommended that the model be validated and calibrated using data from irradiated U_3Si_2. However, the availability of such data, as of the writing of this thesis, is at least three years into the future from currently ongoing irradiations in the ATR reactor at INL. Also, some parameters could be determined more accurately and fixed using a combination of molecular dynamics modeling and *ab initio* theory.

The sensitivity of the model with respect to unknown parameters in U_3Si_2 makes it necessary to use experimental data to estimate those parameters and hence obtain results with a higher level of confidence. However, different working zones can be defined for the pellet in relation to temperature and burnup. Low temperature and high burnup promote grain subdivision, and consequently, high swelling (rim conditions). The rest of the pellet experiences higher temperature, at which grain subdivision is more difficult, but still possible. To prevent fuel restructuring from occurring all along the pellet, the average burnup should be kept below a threshold that the present model is unable to predict without proper estimation of the unknown parameters. A possible practical engineering solution would be operating at average burnup levels lower than the threshold, which is to be determined, and at temperatures as high as possible but without taking the risk for pellet melting beyond some acceptable limit.

It appears that working temperatures above 1200 K may prevent grain subdivision; however precise conclusions cannot be drawn until the model is tuned using experimental data. Also, high thermal conductivity of silicide fuel, beneficial to its safety performance, may keep its temperature below this threshold under realistic operating conditions.

It is possible that grain growth at high temperatures may compensate for the grain size reduction caused by recrystallization. If this were to indeed occur, the swelling would be reduced through decreasing gas migration out of the grain and hence reducing the corresponding influence on bubble formation and growth at grain boundaries. Besides, fission gas release at high temperature could be favorable to reducing swelling if the gases escape the pellet entirely or remain within large pores included inside the pellet,

instead of migrating to grain boundaries within the pellet. However, both phenomena should be further modeled or evaluated in experiments.

If it is ultimately determined that grain subdivision would occur all throughout the depth of the pellet, and not only within a short thickness from its outer surface, then a solution can be proposed. If pores are included within the pellet during manufacturing (e.g., via a process that uses pore formers) [59, 60], they would act as sinks for the gases released from the grains. These pores would already be part of the initial pellet and thus would not cause any additional dimensional change. On the other hand, the content of fissile material in the pellet would be reduced. To consider this solution, the trade-off between the reduction of swelling and the loss of fissile material should be assessed. Besides, the pores would have to survive densification in the reactor and, hence, the critical pore diameter that allows avoidance of pore disappearance during densification must be found. This particular densification and any other shrinking phenomena are known for UO_2, but not for U_3Si_2.

APPENDIX I

Damage modeling

The success of model validation depends to some extent on the accuracy with which the damage caused by collision cascades is modeled. The simplest models consider that the damage to the material occurs as production of Frenkel pairs that are homogeneously distributed in the material volume. However, real damage is produced in a heterogeneous fashion, where each collision cascade defines an inner region with clusters of vacancies and an outer annulus consisting of interstitial clusters; and such a heterogeneous structure persists even after annealing of the thermal spike. Only a fraction of the produced defects can escape the cascade as free migrating defects. Moreover, another fraction of the produced defects recombines during the thermal spike, reducing the effective amount of defects created.

It is hard to fully model this (actual) configuration of the damage, but it is possible to predict the total amount of defects generated and, then, define parameters that determine the fraction of defects that recombine within the thermal spike, the fraction of defects that cluster and the fraction of freely migrating defects. The latter fraction should be the one used for the defects generated per fission event in reaction rate models, such as the model developed in this work.

In the present work, to determine the number of vacancies (and, hence, of interstitial) that are generated, the SRIM code was used. This code uses a binary collision method to

calculate the number of displacements generated by an energetic ion in a given material. This code has the disadvantage of considering the material to be pseudo-amorphous (although a crystalline structure is considered, no crystalline or ionic effects are taken into account) and it neglects any thermal effect (i.e., assumes irradiation is carried out at 0 K).

As the fission fragments, which cause most of the damage in the crystalline structure, are charged particles, their stopping is divided in two steps. First, electronic stopping reduces the particle energy until elastic collision can occur. Then, head-on collisions between atoms displace atoms from the lattice, thus generating the defects. For the production of displacements, it is necessary that the moving atom transfer enough energy to the lattice atom to cause it to overcome the energy barrier to displacement (i.e., the energy imposed on it by the lattice and that would make it stay in place). This energy is named the threshold displacement energy.

To obtain significant values from SRIM, it is important to know the threshold energy for each atom. Several studies have been performed to estimate this value for UO_2. Special attention ought to be given to the work of Meis and Chartier [61]. They found that the threshold displacement energy depends on the crystallographic plane on which the atom is displaced and on the type of atom. In average, the threshold displacement energies are 21 eV for O and 60 eV for U.

Using these values, the amount of defects produced depends, mainly, on the mass of the fission fragment with some slight variations when the energy of the particle changes. It

can be seen that more O^{2-} than U^{4+} defects are produced, which is consistent with the need to maintain electrical neutrality (two O^{2-} displaced per U^{4+} displaced). As the diffusivity of O^{2-} ions is higher than that of U^{4+} ions, it can may be assumed that an excess in the production of oxygen interstitials would quickly diffuse back to compensate for any local electrical unbalance.

If this consideration is added to the recombination of vacancies and interstitials that occurs during the thermal spike, then the resulting amount of defects would be much smaller than the amount calculated by SRIM. The final amount of defects can be expressed as a percentage of the initial amount, leaving that percentage as a degree of freedom that should be consistent with values from the literature.

The output of the SRIM simulations shows a strong dependence on the threshold energies and the mass of the fragment and a slight dependence on the energy. This is expected as the starting energy is reduced by electronic stopping until the fragment reaches the cut-off energy below which elastic scattering happens, while the mass of the projectile and the threshold energies are directly related to the calculation of the displacements. Solving for U_3Si_2, the results were similar as those just discussed about UO_2.

The computed number of displacements ranged from 35000 to 90000 per ion for a variety of combinations of parameters. An average of 62000 displacements is taken as a basis for subsequent model calculations. From these displacements, if one considers an efficiency close to 1%, the number of effective displacements drops to 620 per ion. If two fission fragments are produced in each fission event, then 1200 effective displacements occur

per fission. Then, if this value is needed on a per atom basis, one must multiply the per fission value by the atomic volume. In so doing, the fission rate would be divided by around $2 \times 10^{25} \frac{1}{s.m^3}$ to get the amount of point defects produced per second as

$$\mathrm{Q_v} = Q_i = \frac{\dot{f}}{B} \tag{62}$$

where $\dot{f}$ is the fission rate and Q_v and Q_i is the rate of vacancies and interstitials created per atomic volume, respectively. Then

$$\mathrm{B} = \frac{1}{2\mathrm{D}\Omega} \tag{63}$$

where Ω is the atomic volume and D is the amount of displacements produced per ion. The factor of 2 is included to account for the two ions produced per fission.

Furthermore, assuming that half of the defects remain in clusters and are not available as freely migrating defects, the fission rate would have to be divided by $4 \times 10^{25} \frac{1}{s.m^3}$.

This factor is considerably higher than the one used by other models for grain subdivision, which apparently do not take into consideration the efficiency within the collision cascade.

APPENDIX II

Diameter of cellular dislocation networks

Dislocations are defects that distort the crystal lattice of materials and, consequently, generate stress fields around the dislocation lines. Previous research has proved that dislocations can pack in different arrangements that mutually shield from this stress and thus decrease the per-dislocation energy.

The ultimate stable arrangement is the cellular dislocation network in which dislocations are grouped as walls that delimit subgrains. Generally, these structures appear as subgrain walls with high dislocation density while the interior of the subgrain thus delimited is free of any strain.

The energy of these dislocations is a function of the diameter of the subgrain. Thus, it is possible to obtain an expression for the diameter at which the energy is lowest.

Hansen and Kuhlmann-Wilsdorf [62] developed a theoretical framework to show the relationship between the network dislocation density (ρ_N) and the subgrain diameter (d_N), finding the minimum energy of that structure. The stored energy of the dislocation networks can be divided between the energy of the dislocation and the energy of the dislocation terminations, as defined in equations (64) and (65), respectively.

$$\mathrm{U_D} \approx \rho_N \frac{G b_v^2 f(\nu)}{4\pi} ln(\frac{C_\rho C_A}{d_N \rho_N b_v}) \tag{64}$$

$$\mathrm{U_W} = \frac{G}{2}\left[\frac{b_v f(\nu) d_N \rho_N}{2\pi C_\rho C_A}\right]^2 \tag{65}$$

where G is the shear modulus, b_v is the Burgers vector, $f(\nu)$ is a function of the Poisson Ratio and $C_\rho C_A$ is a parameter that depends on the material.

Both contributions are expressed as a function of the subgrain diameter, thus it is possible to find a critical diameter for which the energy of the dislocation network is minimized by taking the derivative of the sum $\mathrm{U_D} + \mathrm{U_W}$ with respect to the diameter $\mathrm{d_N}$,

$$\frac{\mathrm{d}(\mathrm{U_D} + U_W)}{\mathrm{dd_N}} = G d_N \left[\frac{b_v f(\nu)\rho_N}{2\pi C_\rho C_A}\right]^2 - \rho_N \frac{G b_v^2 f(\nu)}{4\pi d_N} = 0 \tag{66}$$

and solving eq. (66), to get

$$\mathrm{d_N} = C_\rho C_A \sqrt{\frac{\pi}{f(\nu)\rho_N}} \tag{67}$$

The diameter defined here is inversely proportional to the inverse of the square root of the dislocation density. However, the factor $C_\rho C_A$ is not properly defined and its value seems to depend on the material.

Baranov et al. [41] reduced the expression in equation (67) to a more straightforward form

$$\mathrm{d_N} = a\rho_N^b \tag{68}$$

and found that, for UO_2, $\mathrm{b} = -0.5$, consistent with the inverse of the square root of equation (67), and that $\mathrm{a} = 3.5$, which corresponds to a value of $C_\rho C_A = 2.185$. This

result is the one used in the present work, which is lower than the value used by Rest in his works ($C_\rho C_A = 3$).

APPENDIX IV

Preliminary model for microstructural evolution with loop unfaulting

A similar model to the one presented in the main body of the thesis is proposed here as an alternative approach that takes into consideration the intermediate stage of prismatic (or Frank) loops before the dislocations can join the network. To join the network, these loops must first unfault to be able to glide towards the cell wall. The unfaulting process can be autocatalytic or induced by reaction with other dislocations.

Then, clusters grow to become prismatic loops, which grow further or shrink, depending on the conditions. If the prismatic loops grow over a critical diameter, they will unfault and become perfect loops, which may glide.

As Frank loops grow by climb (if coalescence is ignored), the rate at which Frank loops grow over the critical diameter is determined by the following formula:

$$K_{unf} = \frac{\nu_I}{d_{crit} - d} \tag{69}$$

However, the loop size is not unique, rather a distribution of loop sizes would be expected to be present. One could assume that the aforementioned distribution is a truncated normal distribution bounded by the minimum loop size and the critical diameter,

$$p^*(d) = Kp(d), \tag{70}$$

where $p(d)$ is a normal distribution function with a mean value equal to the average loop diameter and a standard deviation to be determined and K is a normalizing factor to account for the truncation. By doing so, one could integrate the unfaulting rate over all the distribution and obtain an instantaneous (weighted) rate,

$$\widetilde{K}_{unf} = \int_{d_{min}}^{d_{crit}} p^*(d_I) \frac{\nu_I}{d_{crit} - d_I} dd_I. \tag{71}$$

Once the Frank loop unfaults and transforms into a perfect loop, it increases the line density of "free" bulk dislocations. These dislocations are then able to glide and join the dislocation network with a rate controlled by climb.

In a similar way, the change in loop size can be evaluated. Considering that the change in diameter due to unfaulting is given by the difference between the initial and final size, it can be averaged over all possible sizes per

$$\Delta \tilde{d}_{I_{unf}} = \frac{\int_{d_{min}}^{d_{crit}} p^*(d) \frac{d_I \nu_I}{d_{crit} - d_I} dd_I}{C_I} \tag{72}$$

Then, the point defect concentration equations are written as

$$\begin{aligned} \frac{dC_v}{dt} = Q_v - K_{iv} C_v C_i - K_{vN}(\rho_N) D_v C_v - K_{vD}(\rho_D) D_v C_v - K_{vL}(\pi C_I d_I) D_v C_v \\ - k_{gb}^2 D_v C_v - 4\pi r_{iv}(D_v + D_{2i}) C_v C_{2i} - \frac{4\pi a_0^2 D_v C_v C_{2i}}{\Omega} \end{aligned} \tag{73}$$

$$\frac{dC_i}{dt} = Q_i - K_{iv}C_vC_i - K_{iN}(\rho_N)D_iC_i - K_{iD}(\rho_D)D_iC_i - K_{iL}(\pi C_I d_I)D_iC_i$$
$$- k_{gb}^2 D_iC_i - 16\pi r_{iv}D_iC_i^2 + 4\pi r_{iv}(D_v + D_{2i})C_vC_{2i} \quad (74)$$
$$- \frac{4\pi a_0^2 D_iC_iC_{2i}}{\Omega}$$

Eq. (73) represents the balance of vacancies concentration where the contribution of the vacancies generation, the recombination with interstitials, the annihilation to dislocations (network dislocations, bulk dislocations and Frank loops), grain boundaries and di-interstitials and reaction with clusters are considered, respectively. Equation (74) represents the balance of interstitials where the generation, the recombination with vacancies, the annihilation to dislocations (network dislocations, bulk dislocations and Frank loops) and grain boundaries, the loss due to formation of di-interstitials, the creation due to reaction of vacancies with di-interstitials and reaction with clusters are listed in that order [1, 27, 48]. These equations are equivalent to equations (17) and (18), respectively.

The diffusion coefficients, the recombination rate and the grain boundary sink strength are calculated as explained in the original model.

K_{jX} is the sink strength of dislocations and can be rewritten as:

$$K_{jX} = Z_{jX}\rho_X \quad (75)$$

with $j = i, v$ and $j = N, D, L$, for interstitials and vacancies and network dislocations, bulk dislocations and loops, respectively. The bias takes different values for loops, bulk dislocations and network dislocations. As loops grow in size, they can be approximated

with higher precision to a straight dislocation, so Z_{jL} approaches Z_{jD} as the loops diameter grows to be infinite. Although, in essence, dislocations in the network are straight dislocations, some difference in their behavior will be explained later.

Values for Z_{jL}, Z_{jN} and Z_{jD} were calculated according to Dubinko et al. [49]. These values are calculated per

$$Z_{jN} = Z_{j0} + 2\sum_{n=1}^{\infty}(-1)^n Z_{jn} \approx Z_{j0} - Z_{j1}, \tag{76}$$

with

$$Z_{jn} = \frac{2\pi I_n\left(\frac{L_j}{2r_0}\right) I_n\left(\frac{L_j}{2R}\right)}{I_n\left(\frac{L_j}{2r_0}\right) K_n\left(\frac{L_j}{2R}\right) - K_n\left(\frac{L_j}{2r_0}\right) I_n\left(\frac{L_j}{2R}\right)}, \tag{77}$$

where I_n and K_n stand for the modified Bessel functions of order n, $R = \frac{1}{\sqrt{\pi\rho_D}}$, r_0 is the core radius of the dislocations, ρ_D is the total dislocation density and

$$L_{v,i} = \left|\frac{1}{3\pi}\frac{(1+\nu)Gb_v\Delta V_{v,i}}{(1-\nu)k_bT}\right|, \tag{78}$$

where $k_b$is the Boltzmann constant, G is the shear modulus, ν is the Poisson ratio, $\Delta V_{v,i}$ stands for the relaxation volume of vacancies and interstitials, respectively. Once the sink strength for straight dislocations is calculated, the sink strength of the loops is obtained from equation (79).

$$Z_{jL} = Z_{jd} + \frac{3.6L_j^{0.255} - Z_{jn}}{\frac{d_I}{2b_v}^{2/3} + 0.2} \tag{79}$$

When calculating R, different dislocation densities are used depending on whether the calculation is being performed for loops and straight dislocations in the interior of the subgrain or is being carried out for network dislocations for the cell wall.

To calculate the concentration (or density) of di-interstitials (C_{2i}), bulk dislocations (ρ_D) and dislocation networks (ρ_N), the following equations are postulated:

$$\frac{d\rho_D}{dt} = \widetilde{K}_{unf} - f_1\beta\frac{|v_D|}{d_N}\rho_D - f_3|v_D|\rho_D^{2/3} + \frac{3}{4}K_{sweep}\pi d_I C_I \tag{80}$$

$$\frac{d\rho_N}{dt} = f_1\beta\frac{|v_D|}{d_N}\rho_D - f_2\eta\frac{|v_N|}{d_N}\rho_N \tag{81}$$

$$\frac{dC_{2i}}{dt} = Q_{2i} + 8\pi\frac{r_{iv}D_iC_i^2}{\Omega^2} - 4\pi\frac{r_{iv}D_iC_vC_{2i}}{\Omega} - \frac{\pi\nu_{2i}c_{2i}}{b_v} - K_{resol} - K_{abs} \tag{82}$$

Equations (80), (81) and (82) are the balances for the bulk dislocation density, the dislocation network density and di-interstitial concentration, respectively. ν_I stands for the dislocation climb, which is considered the limiting mobility mechanism for dislocations [37]. Dislocation networks are generated by pilling up of bulk dislocation and annihilated by recombination with an opposite dislocation. Di-interstitials are generated in collision cascades and by combination of two interstitials, destroyed by reaction with a vacancy, and can grow by climb.

In equations (80) and (81), f_1, f_2 and f_3 are geometric factors that have not been properly modeled in this work and will be estimated, while β is a factor that takes into account the back-stress suffered by the dislocation moving towards the network from the dislocations that are already in the network. This factor could be a constant or could depend on other

variables, however its modeling is out of the scope of this work and the following approximation is used:

$$\beta = \sqrt{\frac{10^{15} m^{-2}}{\rho_N}} \tag{83}$$

The factor η from equation (81) affects the annihilation of the dislocation in the network to account for the decrease in the efficiency of climb in a region of tangled dislocations. As climb feeds from point defects arriving to the dislocations, a region of high density of dislocations will reduce the effective flux of point defects. The following extremely simplified expression was used:

$$\eta = \sqrt{\frac{10^{13} m^{-2}}{\rho_N}} \tag{84}$$

In equation (80), K_{sweep}represents the increase of the linear dislocation density due to the unfaulting of prismatic loops when they are swept by gliding dislocations [63]. The expression used is

$$K_{sweep} = \frac{f_3 \nu_D}{\sqrt{\rho_D}} \tag{85}$$

In equation (82), K_{resol} stands for the rate of re-solution of clusters due to radiation cascades, while K_{abs} is the rate at which clusters are captured by dislocations. For the former rate, it is considered that clusters inside the fission track volume are destroyed; for the latter, it is assumed that the absorption of clusters by dislocations is activated by the absorption of a single interstitial. Hence, the following expressions are obtained:

$$K_{resol} = 2fV_t \tag{86}$$

$$K_{abs} = [K_{iD}(\rho_D)D_iC_i + K_{iL}(\pi C_I d_I)D_iC_i](\rho_D + \pi C_I d_I)\pi\left(\frac{L_i}{2}\right)^2 C_{2i} \tag{87}$$

Equation (87) can be explained in the following way; clusters are homogeneously distributed in space and some of them are contained within the range of dislocations, when an interstitial is absorbed by a dislocation with a cluster next to it, the cluster get absorbed too.

The intermediary between defects generated by radiation and dislocations arranging into cell walls are the prismatic (or Frank) interstitial loops. Special attention is paid to them as they do not behave similarly to the other species. Frank loops are characterized by an average concentration and by an average loop diameter. As it has been explained above, these loops will unfault when attaining a critical radius given by the stacking fault energy. However, it is necessary to obtain an unfaulting rate for the loops. This rate is calculated assuming a normal distribution of the loops, as detailed in equation (71).

Then, the loop concentration (C_I) and its average diameter (d_I) are calculated as follows:

$$\frac{dC_I}{dt} = \frac{\pi\nu_{2i}C_{2i}}{2a_0} - \widetilde{K}_{unf}C_I - 8\nu_I d_I^2 C_I^2 - K_{sweep} \tag{88}$$

$$\frac{d(d_I)}{dt} = \nu_I^* - (d_I - 2a_0)\frac{\dot{C_{2i\to I}}}{C_I} + d_I\frac{\dot{C_{2I\to I_2}}}{C_I} - \Delta\tilde{d}_{I_{unf}} \tag{89}$$

$$\dot{C_{2i\to I}} = \frac{\pi\nu_{2i}c_{2i}}{2a_0} \tag{90}$$

$$\dot{C_{2I\to I_2}} = 8\nu_I d_I^2 C_I^2 \tag{91}$$

Except for the first and last terms in the time evolution of the average loop diameter, the rest of the terms are calculated using the same reasoning as in the main model.

The concentration of interstitial prismatic loops increases due to growth of di-interstitials (and clusters) and decreases when they unfault and become perfect loops (equation (72)) or when two loops coalesce (Equation (88)). Its diameter can increase or decrease through climb, decreases when smaller than average size loops are formed from di-interstitials (Equation (89)) or when loops unfault and increases when loops coalesce.

Validation with α-doped UO_2

To start defining parameter of the model, it will be tested against data from α-doped UO_2 at room temperature. The experimental data used to validate the model are taken from Jérome Jonnet's doctoral thesis [64] and from a paper he later published together with other authors [55].

Samples were prepared using a sol-gel technique to obtain a solid solution of UO_2 with 10% Pu. These samples were left to self-irradiate during a long period of time (4 and 7 years) until the decay of the Pu produced enough damage to the material. After the irradiation time terminated, samples were analyzed using TEM imaging. The microstructure was predominantly composed of interstitial loops. Size distributions for the loops were obtained.

These data provide an adequate basis to validate the loop formation and growth, although the low temperature and low "fission density equivalent" prevent further evolution of the microstructure. Results from the present analysis were consistent with the experimental data.

APPENDIX V

FASTGRASS Sensitivity Analysis

Due to the large number of parameters on which FASTGRASS relies, it was important to detect the ones that caused the largest change by modifying them through reasonable ranges of values.

Table 6. Summary of FASTGRASS relevant parameters.

Parameter	Description	Table
BVCRIT	Critical value of grain edge swelling required for long-range tunnel interlinkage.	Table 7
SIGPI	Width of distribution of grain edge porosity interlinkage probability.	Table 8
ASTAR	Fraction of areal coverage of grain face by bubbles required for channel formation.	Table 9
SBCF	Width of distribution of grain-face channel formation probability.	Table 10
RESCON	Re-solution constant.	Table 11
GBR(1)	Multiplies RESCON to obtain effective irradiation-induced re-solution of gas atoms from grain face.	Table 12
GBR(2)	Multiplies RESCON to obtain effective irradiation-induced re-solution of gas atoms from grain edge.	Table 13
REDIS	Average distance traveled by an atom ejected from a grain boundary bubble.	Table 14

This analysis was performed by coding a batch file with the capacity of running a large number of FASTGRASS simulations with different input decks. Each parameter

variation was simulated for different temperatures, grain sizes and fission rates (by changing the linear power).

Results from these simulations were transferred to tables. The description of the parameters varied is summarized in Table 6.

Table 7. Variations in swelling due to changes in BVCRIT.

BVCRIT	Grain size (cm)	Lin. Pow. (kW/ft)	700 K		900 K		1500 K	
5.50E-02	3.00E-03	6.67	1	3.49E-02	7	3.53E-02	13	6.37E-02
		11.67	2	6.11E-02	8	6.18E-02	14	1.09E-01
	3.00E-04	6.67	3	3.52E-02	9	3.67E-02	15	1.35E-01
		11.67	4	6.12E-02	10	6.31E-02	16	1.38E-01
	3.00E-05	6.67	5	3.63E-02	11	4.36E-02	17	4.53E-01
		11.67	6	4.86E-02	12	5.24E-02	18	4.93E-01
5.50E-01	3.00E-03	6.67	19	3.49E-02	25	3.53E-02	31	6.53E-02
		11.67	20	6.11E-02	26	6.18E-02	32	1.21E-01
	3.00E-04	6.67	21	3.54E-02	27	3.68E-02	33	4.58E-01
		11.67	22	6.16E-02	28	6.36E-02	34	5.90E-01
	3.00E-05	6.67	23	1.03E-01	29	1.28E-01	35	4.53E-01
		11.67	24	3.09E-01	30	4.58E-01	36	9.43E-01
9.00E-01	3.00E-03	6.67	37	3.49E-02	43	3.53E-02	49	6.53E-02
		11.67	38	6.11E-02	44	6.18E-02	50	1.21E-01
	3.00E-04	6.67	39	3.54E-02	45	3.68E-02	51	4.58E-01
		11.67	40	6.16E-02	46	6.36E-02	52	7.28E-01
	3.00E-05	6.67	41	1.03E-01	47	1.28E-01	53	4.53E-01
		11.67	42	3.09E-01	48	4.58E-01	54	9.79E-01

Table 8. Variations in swelling due to changes in SIGPI.

SIGPI	Grain size (cm)	Lin. Pow. (kW/ft)	700 K		900 K		1500 K	
2.00E-03	3.00E-03	6.67	1	3.49E-02	7	3.53E-02	13	6.53E-02
		11.67	2	6.11E-02	8	6.18E-02	14	6.05E-02
	3.00E-04	6.67	3	3.54E-02	9	3.68E-02	15	3.49E-02
		11.67	4	6.16E-02	10	6.36E-02	16	6.08E-02
	3.00E-05	6.67	5	1.03E-01	11	1.28E-01	17	3.65E-02
		11.67	6	3.09E-01	12	4.58E-01	18	6.39E-02
2.00E-01	3.00E-03	6.67	19	3.49E-02	25	3.53E-02	31	3.45E-02
		11.67	20	6.11E-02	26	6.18E-02	32	6.05E-02
	3.00E-04	6.67	21	3.53E-02	27	3.68E-02	33	3.48E-02
		11.67	22	6.15E-02	28	6.34E-02	34	6.07E-02
	3.00E-05	6.67	23	1.01E-01	29	1.25E-01	35	3.60E-02
		11.67	24	2.60E-01	30	3.15E-01	36	6.15E-02
5.00E-02	3.00E-03	6.67	37	3.49E-02	43	3.53E-02	49	3.45E-02
		11.67	38	6.11E-02	44	6.18E-02	50	6.05E-02
	3.00E-04	6.67	39	3.54E-02	45	3.68E-02	51	3.49E-02
		11.67	40	6.16E-02	46	6.36E-02	52	6.08E-02
	3.00E-05	6.67	41	1.03E-01	47	1.28E-01	53	3.65E-02
		11.67	42	3.08E-01	48	4.35E-01	54	6.39E-02

Table 9. Variations in swelling due to changes in ASTAR.

ASTAR	Grain size (cm)	Lin. Pow. (kW/ft)	700 K		900 K		1500 K	
8.00E-01	3.00E-03	6.67	1	3.49E-02	7	3.53E-02	13	6.19E-02
		11.67	2	6.11E-02	8	6.18E-02	14	1.27E-01
	3.00E-04	6.67	3	3.54E-02	9	3.68E-02	15	4.57E-01
		11.67	4	6.16E-02	10	6.36E-02	16	5.83E-01
	3.00E-05	6.67	5	1.04E-01	11	1.29E-01	17	4.53E-01
		11.67	6	3.13E-01	12	3.95E-01	18	1.10E+00
6.50E-01	3.00E-03	6.67	19	3.49E-02	25	3.53E-02	31	5.97E-02
		11.67	20	6.11E-02	26	6.18E-02	32	1.17E-01
	3.00E-04	6.67	21	3.54E-02	27	3.68E-02	33	4.51E-01
		11.67	22	6.17E-02	28	6.36E-02	34	5.74E-01
	3.00E-05	6.67	23	1.05E-01	29	1.31E-01	35	5.77E-01
		11.67	24	2.94E-01	30	4.49E-01	36	7.51E-01
5.00E-01	3.00E-03	6.67	37	3.49E-02	43	3.53E-02	49	5.99E-02
		11.67	38	6.11E-02	44	6.18E-02	50	1.17E-01
	3.00E-04	6.67	39	3.54E-02	45	3.69E-02	51	4.12E-01
		11.67	40	6.17E-02	46	6.36E-02	52	5.65E-01
	3.00E-05	6.67	41	1.06E-01	47	1.32E-01	53	6.15E-01
		11.67	42	2.96E-01	48	4.26E-01	54	8.10E-01

Table 10. Variations in swelling due to changes in SBCF.

SBCF	Grain size (cm)	Lin. Pow. (kW/ft)	700 K		900 K		1500 K	
5.00E+02	3.00E-03	6.67	1	3.49E-02	7	3.53E-02	13	5.99E-02
		11.67	2	6.11E-02	8	6.18E-02	14	1.17E-01
	3.00E-04	6.67	3	3.54E-02	9	3.68E-02	15	4.24E-01
		11.67	4	6.16E-02	10	6.36E-02	16	5.79E-01
	3.00E-05	6.67	5	3.76E-02	11	3.88E-02	17	4.53E-01
		11.67	6	6.59E-02	12	7.75E-02	18	8.49E-01
1.00E+01	3.00E-03	6.67	19	3.49E-02	25	3.53E-02	31	6.50E-02
		11.67	20	6.11E-02	26	6.18E-02	32	1.29E-01
	3.00E-04	6.67	21	9.81E-02	27	2.62E-01	33	4.14E-01
		11.67	22	1.58E-01	28	5.30E-01	34	5.92E-01
	3.00E-05	6.67	23	1.61E-01	29	3.94E-01	35	4.53E-01
		11.67	24	3.07E-01	30	4.99E-01	36	9.43E-01
5.00E+01	3.00E-03	6.67	37	3.49E-02	43	3.53E-02	49	6.15E-02
		11.67	38	6.11E-02	44	6.18E-02	50	1.25E-01
	3.00E-04	6.67	39	3.54E-02	45	3.68E-02	51	4.55E-01
		11.67	40	6.16E-02	46	6.59E-02	52	5.90E-01
	3.00E-05	6.67	41	1.60E-01	47	2.23E-01	53	4.53E-01
		11.67	42	3.00E-01	48	5.17E-01	54	9.43E-01

Table 11. Variations in swelling due to changes in RESCON.

RESCON	Grain size (cm)	Lin. Pow. (kW/ft)	700 K		900 K		1500 K	
2.00E-18	3.00E-03	6.67	1	3.50E-02	7	3.54E-02	13	6.43E-02
		11.67	2	6.12E-02	8	6.19E-02	14	1.20E-01
	3.00E-04	6.67	3	3.60E-02	9	2.03E-01	15	3.73E-01
		11.67	4	6.29E-02	10	6.70E-02	16	6.26E-01
	3.00E-05	6.67	5	3.77E-02	11	4.11E-01	17	5.32E-01
		11.67	6	6.61E-02	12	9.87E-02	18	9.60E-01
2.00E-16	3.00E-03	6.67	19	3.47E-02	25	3.50E-02	31	4.74E-02
		11.67	20	6.10E-02	26	6.16E-02	32	7.68E-02
	3.00E-04	6.67	21	3.48E-02	27	3.52E-02	33	1.98E-01
		11.67	22	6.10E-02	28	6.17E-02	34	3.87E-01
	3.00E-05	6.67	23	1.30E-01	29	2.86E-01	35	5.11E-01
		11.67	24	2.49E-01	30	5.10E-01	36	8.27E-01
2.00E-15	3.00E-03	6.67	37	3.47E-02	43	3.50E-02	49	3.61E-02
		11.67	38	6.07E-02	44	6.12E-02	50	6.31E-02
	3.00E-04	6.67	39	3.47E-02	45	3.50E-02	51	4.20E-02
		11.67	40	6.07E-02	46	6.12E-02	52	7.26E-02
	3.00E-05	6.67	41	6.41E-02	47	2.56E-01	53	2.24E-01
		11.67	42	1.23E-01	48	4.90E-01	54	5.03E-01

Table 12. Variations in swelling due to changes in GBR(1).

GBR(1)	Grain size (cm)	Lin. Pow. (kW/ft)	700 K		900 K		1500 K	
2.00E-02	3.00E-03	6.67	1	3.49E-02	7	3.53E-02	13	3.91E-02
		11.67	2	6.11E-02	8	6.17E-02	14	7.24E-02
	3.00E-04	6.67	3	3.49E-02	9	3.53E-02	15	4.30E-02
		11.67	4	6.11E-02	10	6.18E-02	16	7.65E-02
	3.00E-05	6.67	5	9.97E-02	11	2.07E-01	17	2.18E-01
		11.67	6	2.60E-01	12	3.45E-01	18	5.64E-01
2.00E-03	3.00E-03	6.67	19	3.49E-02	25	3.53E-02	31	5.02E-02
		11.67	20	6.11E-02	26	6.18E-02	32	9.77E-02
	3.00E-04	6.67	21	3.51E-02	27	3.62E-02	33	2.79E-01
		11.67	22	6.15E-02	28	6.22E-02	34	5.68E-01
	3.00E-05	6.67	23	1.01E-01	29	1.26E-01	35	4.99E-01
		11.67	24	3.06E-01	30	3.92E-01	36	8.30E-01
2.00E-05	3.00E-03	6.67	37	3.49E-02	43	3.53E-02	49	6.72E-02
		11.67	38	6.11E-02	44	6.18E-02	50	1.34E-01
	3.00E-04	6.67	39	3.54E-02	45	2.73E-01	51	4.60E-01
		11.67	40	6.17E-02	46	6.36E-02	52	6.12E-01
	3.00E-05	6.67	41	1.03E-01	47	4.10E-01	53	5.32E-01
		11.67	42	3.09E-01	48	4.12E-01	54	1.04E+00

Table 13. Variations in swelling due to changes in GBR(2).

GBR(2)	Grain size (cm)	Lin. Pow. (kW/ft)	700 K		900 K		1500 K	
2.00E-02	3.00E-03	6.67	1	3.49E-02	7	3.53E-02	13	4.36E-02
		11.67	2	6.11E-02	8	6.18E-02	14	7.64E-02
	3.00E-04	6.67	3	3.49E-02	9	3.53E-02	15	1.47E-01
		11.67	4	6.11E-02	10	6.18E-02	16	1.67E-01
	3.00E-05	6.67	5	7.00E-02	11	3.32E-01	17	4.53E-01
		11.67	6	1.29E-01	12	4.88E-01	18	8.37E-01
2.00E-03	3.00E-03	6.67	19	3.49E-02	25	3.53E-02	31	5.15E-02
		11.67	20	6.11E-02	26	6.18E-02	32	9.84E-02
	3.00E-04	6.67	21	3.49E-02	27	3.53E-02	33	3.19E-01
		11.67	22	6.12E-02	28	6.18E-02	34	4.72E-01
	3.00E-05	6.67	23	1.33E-01	29	2.96E-01	35	4.53E-01
		11.67	24	2.52E-01	30	5.10E-01	36	1.13E+00
2.00E-05	3.00E-03	6.67	37	3.49E-02	43	3.54E-02	49	6.66E-02
		11.67	38	6.12E-02	44	6.20E-02	50	1.28E-01
	3.00E-04	6.67	39	3.64E-02	45	4.03E-02	51	4.66E-01
		11.67	40	6.36E-02	46	7.00E-02	52	5.86E-01
	3.00E-05	6.67	41	3.77E-02	47	4.42E-02	53	4.53E-01
		11.67	42	6.61E-02	48	9.87E-02	54	9.32E-01

Table 14. Variations in swelling due to changes in REDIS.

REDIS	Grain size (cm)	Lin. Pow. (kW/ft)	700 K		900 K		1500 K	
1.00E-06	3.00E-03	6.67	1	3.49E-02	7	3.53E-02	13	6.22E-02
		11.67	2	6.11E-02	8	6.18E-02	14	1.11E-01
	3.00E-04	6.67	3	3.54E-02	9	3.68E-02	15	3.62E-01
		11.67	4	6.16E-02	10	6.36E-02	16	5.87E-01
	3.00E-05	6.67	5	1.60E-01	11	1.94E-01	17	4.28E-01
		11.67	6	2.90E-01	12	5.09E-01	18	9.08E-01
1.00E-07	3.00E-03	6.67	19	3.49E-02	25	3.53E-02	31	6.65E-02
		11.67	20	6.11E-02	26	6.18E-02	32	1.22E-01
	3.00E-04	6.67	21	3.54E-02	27	3.72E-02	33	4.49E-01
		11.67	22	6.16E-02	28	6.36E-02	34	6.04E-01
	3.00E-05	6.67	23	5.00E-02	29	5.54E-02	35	5.09E-01
		11.67	24	1.86E-01	30	2.33E-01	36	1.02E+00
1.00E-08	3.00E-03	6.67	37	3.50E-02	43	3.54E-02	49	7.23E-02
		11.67	38	6.12E-02	44	6.19E-02	50	1.33E-01
	3.00E-04	6.67	39	3.56E-02	45	3.79E-02	51	2.74E-01
		11.67	40	6.20E-02	46	6.58E-02	52	4.72E-01
	3.00E-05	6.67	41	3.77E-02	47	4.42E-02	53	5.82E-01
		11.67	42	7.34E-02	48	9.88E-02	54	1.02E+00

REFERENCES

1. Rest, J. and G.L. Hofman, *Dynamics of irradiation-induced grain subdivision and swelling in U_3Si_2 and UO_2 fuels.* Journal of Nuclear Materials, 1994. **210**(1–2): p. 187-202.

2. Petrovic, B., *Integral Inherently Safe Light Water Reactor (I2S-LWR) – Concept Overview*, in *2013 ANS Winter Meeting*. 2013: Washington, DC.

3. Petrovic, B. *Integral Inherently Safe Light Water Reactor (I2S-LWR) Concept: Extending SMR Safety Features to Large Power Output* in *ICAPP 2014*. 2014. Charlotte, USA.

4. S. Ray, E.L., F. Franceschini, *ASSESSMENT OF DIFFERENT MATERIALS FOR MEETING THE REQUIREMENT OF FUTURE FUEL DESIGNS*, in *2012 Reactor Fuel Performance Meeting*. 2012: Manchester, UK.

5. Callister, W.D., *Fundamentals of Materials Science and Engineering.* 2001.

6. Kim, K.H., et al., *Characteristics of U3Si and U3Si2 Powders Prepared by Centrifugal Atomization.* Journal of Nuclear Science and Technology, 1997. **34**(12): p. 1127-1132.

7. Hofman, G.L., *Crystal structure stability and fission gas swelling in intermetallic uranium compounds.* Journal of Nuclear Materials, 1986. **140**(3): p. 256-263.

8. Zachariasen, W., *Crystal chemical studies of the 5f-series of elements. I. New structure types.* Acta Crystallographica, 1948. **1**(5): p. 265-268.

9. Zachariasen, W., *Crystal chemical studies of the 5f-series of elements. VIII. Crystal structure studies of uranium silicides and of CeSi2, NpSi2, and PuSi2.* Acta Crystallographica, 1949. **2**(2): p. 94-99.

10. Was, G.S., *Fundamentals of Radiation Materials Science*. 2007: Springer.

11. Sizmann, R., *The effect of radiation upon diffusion in metals.* Journal of Nuclear Materials, 1978. **69–70**(0): p. 386-412.

12. Kinchin, G.H. and R.S. Pease, *The Displacement of Atoms in Solids by Radiation.* Reports on Progress in Physics, 1955. **18**(1): p. 1.

13. Semenov, A.A. and C.H. Woo, *Classical nucleation theory of microstructure development under cascade-damage irradiation.* Journal of Nuclear Materials, 2003. **323**(2–3): p. 192-204.

14. Kojima, S., et al., *Fluctuation effect of point defect reaction on nucleation of interstitial clusters during neutron irradiation.* Journal of Nuclear Materials, 1992. **191–194, Part B**: p. 1155-1159.

15. Veyssiere, P. and J. Rabier, *COMPUTATIONS OF STACKING FAULT ENERGIES IN IONIC CRYSTALS.* Le Journal de Physique Colloques, 1974. **35**(C7): p. C7-97-C7-101.

16. Nogita, K. and K. Une, *Radiation-induced microstructural change in high burnup UO2 fuel pellets.* Nuclear Instruments and Methods in Physics Research Section B: Beam Interactions with Materials and Atoms, 1994. **91**(1–4): p. 301-306.

17. Doherty, R.D. and R.W. Cahn, *Nucleation of new grains in recrystallization of cold-worked metals.* Journal of the Less Common Metals, 1972. **28**(2): p. 279-296.

18. Rios, P.R., et al., *Nucleation and growth during recrystallization.* Materials Research, 2005. **8**: p. 225-238.

19. Zinkle, S.J., G.L. Kulcinski, and L.K. Mansur, *Radiation-enhanced recrystallization in copper alloys.* Journal of Nuclear Materials, 1986. **141–143, Part 1**(0): p. 188-192.

20. Hagrman, D.L. and G.A. Reymann, *MATPRO-Version 11: a handbook of materials properties for use in the analysis of light water reactor fuel rod behavior*. 1979. p. Medium: ED.

21. Rest, J., *Modeling of Fission-Gas-Induced Swelling of Nuclear Fuels*, in *Comprehensive Nuclear Materials*, R.J.M. Konings, Editor. 2012, Elsevier: Oxford. p. 579-627.

22. Olander, D.R., *Fundamental aspects of nuclear reactor fuel elements: prepared for the Division of Reactor Development and Demonstration, Energy Research and Development Administration*. 1976: Technical Information Center, Office of Public Affairs, Energy Research and Development Administration.

23. Laboratory, O.R.N., *GRASS-SST: Code System to Predict Fission-Gas Release & Fuel Swelling*, RSICC, Editor.

24. Rest, J. and S.A. Zawadzki, *FASTGRASS: A mechanistic model for the prediction of Xe, I, Cs, Te, Ba, and Sr release from nuclear fuel under normal and severe-accident conditions*. 1992: United States. p. 175.

25. Rest, J., *The DART dispersion analysis research tool: A mechanistic model for predicting fission-product-induced swelling of aluminum dispersion fuels. User`s guide for mainframe, workstation, and personal computer applications*, in *Other Information: PBD: Aug 1995*. 1995. p. Medium: ED; Size: 102 p.

26. Matzke, H., *On the rim effect in high burnup UO_2LWR fuels.* Journal of Nuclear Materials, 1992. **189**(1): p. 141-148.

27. Kinoshita, M., *Towards the mathematical model of rim structure formation.* Journal of Nuclear Materials, 1997. **248**(0): p. 185-190.

28. Rest, J., *Derivation of analytical expressions for the network dislocation density, change in lattice parameter, and for the recrystallized grain size in nuclear fuels.* Journal of Nuclear Materials, 2006. **349**(1–2): p. 150-159.

29. Baron, D., et al. *Discussion about hbs transformation in high burn up fuels*. in *Water Reactor Fuel Performance Meeting 2008*. 2008. Korea, Republic of: KNS.

30. Finlay, M.R., et al. *Behaviour of irradiated uranium silicide fuel revisited*. in *2002 International Meeting on Reduced Enrichment for Research and Test Reactors*. 2002. San Carlos de Bariloche, Argentina.

31. Rest, J., *A generalized model for radiation-induced amorphization and crystallization of U_3Si and U_3Si_2 and recrystallization of UO_2.* Journal of Nuclear Materials, 1997. **240**(3): p. 205-214.

32. Rest, J., *Application of a mechanistic model for radiation-induced amorphization and crystallization of uranium silicide to recrystallization of UO_2.* Journal of Nuclear Materials, 1997. **248**(0): p. 180-184.

33. Metzger, K.E., T.W. Knight, and R.L. Williamson, *Model of U3Si2 Fuel System Using BISON Fuel Code*, in *Proceedings of ICAPP 2014*. 2014: Charlotte, USA.

34. Finlay, M.R., G.L. Hofman, and J.L. Snelgrove, *Irradiation behaviour of uranium silicide compounds.* Journal of Nuclear Materials, 2004. **325**(2–3): p. 118-128.

35. ISO, *ISO 15646:2014: Re-sintering test for UO2, (U,Gd)O2 and (U,Pu)O2 pellets*. 2014.

36. Birtcher, R.C. and L.M. Wang, *Stability of uranium silicides during high energy ion irradiation*. 1991: United States. p. 7.

37. Rest, J., *A model for the influence of microstructure, precipitate pinning and fission gas behavior on irradiation-induced recrystallization of nuclear fuels.* Journal of Nuclear Materials, 2004. **326**(2–3): p. 175-184.

38. Rest, J., *A model for the effect of the progression of irradiation-induced recrystallization from initiation to completion on swelling of UO2 and U–10Mo nuclear fuels.* Journal of Nuclear Materials, 2005. **346**(2–3): p. 226-232.

39. Lassmann, K., et al., *Modelling the high burnup UO_2 structure in LWR fuel.* Journal of Nuclear Materials, 1995. **226**(1–2): p. 1-8.

40. Nogita, K. and K. Une, *Irradiation-induced recrystallization in high burnup UO2 fuel.* Journal of Nuclear Materials, 1995. **226**(3): p. 302-310.

41. Baranov, V.G., et al., *Interaction of dislocations in UO_2 during high burn-up structure formation.* Journal of Nuclear Materials, 2014. **444**(1–3): p. 129-137.

42. Walker, C.T., et al., *Concerning the microstructure changes that occur at the surface of UO_2 pellets on irradiation to high burnup.* Journal of Nuclear Materials, 1992. **188**(0): p. 73-79.

43. Cunningham, M.E., M.D. Freshley, and D.D. Lanning, *Development and characteristics of the rim region in high burnup UO2 fuel pellets.* Journal of Nuclear Materials, 1992. **188**(0): p. 19-27.

44. Thomas, L.E., C.E. Beyer, and L.A. Chariot, *Microstructural analysis of LWR spent fuels at high burnup.* Journal of Nuclear Materials, 1992. **188**(0): p. 80-89.

45. Une, K., et al., *Microstructural change and its influence on fission gas release in high burnup UO2 fuel.* Journal of Nuclear Materials, 1992. **188**(0): p. 65-72.

46. Ray, I.L.F., H. Thiele, and H. Matzke, *Transmission electron microscopy study of fission product behaviour in high burnup UO2*, in *Nuclear Materials for Fission Reactors*, H.M. Schumacher, Editor. 1992, Elsevier: Oxford. p. 90-95.

47. Rest, J. and G.L. Hofman, *An alternative explanation for evidence that xenon depletion, pore formation, and grain subdivision begin at different local burnups.* Journal of Nuclear Materials, 2000. **277**(2–3): p. 231-238.

48. Kagana, G. and J. Rest, *A Physical Description of Fission Product Behavior in Fuels for Advanced Power Reactors*, in *ANL-07/24*. 2007, Argonne National Laboratory.

49. Dubinko, V.I., A.S. Abyzov, and A.A. Turkin, *Numerical evaluation of the dislocation loop bias.* Journal of Nuclear Materials, 2005. **336**(1): p. 11-21.

50. Sandström, R., *On recovery of dislocations in subgrains and subgrain coalescence.* Acta Metallurgica, 1977. **25**(8): p. 897-904.

51. Kassner, M. and M.-T. Pérez-Prado, *Five-power-law creep in single phase metals and alloys.* Progress in Materials Science, 2000. **45**(1): p. 1-102.

52. Kroupa, F., *Circular edge dislocation loop.* Cechoslovackij fiziceskij zurnal B, 1960. **10**(4): p. 284-293.

53. Johnson, R.A. and N.Q. Lam, *Solute segregation in metals under irradiation.* Physical Review B, 1976. **13**(10): p. 4364-4375.

54. Spino, J., K. Vennix, and M. Coquerelle, *Detailed characterisation of the rim microstructure in PWR fuels in the burn-up range 40-67 GWd/tM.* Journal of Nuclear Materials, 1996. **231**(3): p. 179-190.

55. Jonnet, J., et al., *Growth mechanisms of interstitial loops in α-doped UO2 samples.* Nuclear Instruments and Methods in Physics Research Section B: Beam Interactions with Materials and Atoms, 2008. **266**(12–13): p. 3008-3012.

56. Shimizu, H., *THE PROPERTIES AND IRRADIATION BEHAVIOR OF U3Si2*. 1965. p. Medium: ED; Size: Pages: 46.

57. Bender, O. and P. Ehrhart, *Self-interstitial atoms, vacancies and their agglomerates in electron-irradiated nickel investigated by diffuse scattering of X-rays.* Journal of Physics F: Metal Physics, 1983. **13**(5): p. 911.

58. Kim, Y.S., *Uranium Intermetallic Fuels (U–Al, U–Si, U–Mo)*, in *Comprehensive Nuclear Materials*, R.J.M. Konings, Editor. 2012, Elsevier: Oxford. p. 391-422.

59. Radford, K.C. and J.M. Pope, *Controlled porosity reactor fuel.* Journal of Nuclear Materials, 1977. **64**(3): p. 289-299.

60. Suryanarayana, S., et al., *Fabrication of UO2 pellets by gel pelletization technique without addition of carbon as pore former.* Journal of Nuclear Materials, 1996. **230**(2): p. 140-147.

61. Meis, C. and A. Chartier, *Calculation of the threshold displacement energies in UO2 using ionic potentials.* Journal of Nuclear Materials, 2005. **341**(1): p. 25-30.

62. Hansen, N. and D. Kuhlmann-Wilsdorf, *Low energy dislocation structures due to unidirectional deformation at low temperatures.* Materials Science and Engineering, 1986. **81**(0): p. 141-161.

63. Gelles, D.S., *A Frank loop unfaulting mechanism in fcc metals during neutron irradiation*. 1981, United Kingdom: Pergamon Press.

64. Jonnet, J., *A contribution to the understanding of the High Burn-up Structure formation in nuclear fuels*. 2007.